Observed changes to the stability of a subsea pipeline caused by seabed mobility

Accepted by *Ocean Engineering* on 31/07/2018

Figures: 18, Words: 8242

Keywords: Pipeline embedment, on-bottom stability, pipe-soil interaction, scour, sediment transport, self-burial, free span

Simon H. F. Leckie
Corresponding author
GHD
Perth, WA 6000
Australia
Phone +61 4 2467 947
Email: simon.leckie@ghd.com
Formerly of The University of Western Australia
Scott Draper
School of Civil, Environmental and Mining Engineering
The University of Western Australia,
Crawley, WA 6009,
Australia
David J. White
Engineering and the Environment
University of Southampton,
University Road
Southampton SO17 1BJ
United Kingdom
Formerly of The University of Western Australia
Liang Cheng
School of Civil, Environmental and Mining Engineering
The University of Western Australia,
Crawley, WA 6009,
Australia
Terry Griffiths
Centre for Offshore Foundation Systems
The University of Western Australia,
Crawley, WA 6009,
Australia
Antonino Fogliani
School of Civil, Environmental and Mining Engineering
The University of Western Australia,
Crawley, WA 6009,
Australia

ABSTRACT

High resolution bathymetry combined with structural modelling is used to estimate changes in the on-bottom stability of an offshore pipeline due to scour and sedimentation over an 11 year period. Detailed observations of post-lay embedment changes have been combined with the pipeline structural characteristics and an elastic-plastic model of soil resistance to estimate the vertical and horizontal stability of the pipeline using a finite difference solution to the beam bending equation. Application of the design approach indicates that post-lay increases to the critical (break-out) velocity of 1 – 2 m/s occur along the full 19 km of surveyed pipeline due to scour and sedimentation, which act to reduce load and increase soil resistance. The rate at which this increase in stability occurs with time is found to vary along the pipeline, and is dependent on the mechanism of pipeline lowering (i.e. whether the pipe lowered due to sagging into widely spaced scour holes, or by sinking into the shoulders between many closely spaced scour holes). By incorporating sediment transport into the pipeline design, the present results suggest potential for significant improvements in pipeline on-bottom stability and associated reductions in minimum required specific gravity and/or secondary stabilisation.

1 INTRODUCTION

Sediment mobility and, in particular, scour around pipelines has been an area of significant research effort for several decades; see, for example, the summaries provided in Sumer and Fredsøe (2002) and Whitehouse (1998). Despite this work and more applied studies (such as the work of Hulsbergen and Bijker (1989) on spoilers), the influence of sediment mobility on pipeline stability design has only been acknowledged in industry codes relatively recently (Det Norske Veritas, 2011). This acknowledgement corrects the erroneous assumption made in more traditional pipeline stability design that a pipeline on a mobile seabed will become unstable before the seabed itself becomes mobile (Palmer, 1996). However, the recent additions do not yet extend to specific guidance on how to predict changes to pipeline embedment due to sediment mobility, or how to make allowance for the associated changes in on-bottom stability in practise.

Recent and ongoing research aims to address this shortcoming. The present paper is part of a wider research effort in which ocean-pipeline-seabed interaction has been studied in a cross-disciplinary manner, combining hydrodynamic, sediment transport and geotechnical expertise (White et al., 2014). The overarching aim is to provide a balanced perspective on pipeline stability, giving seabed mobility due prominence in the work. Draper et al. (2015), for example, present the results of recent physical modelling tests using a unique recirculating flume (described in An et al. (2013)) to simulate scour-induced changes in pipeline stability and their sensitivity to the flow conditions, particularly the change in velocities during the development of a storm.

One of the key barriers to accommodating sediment mobility in pipeline design is that pipeline scour and sedimentation research is predominantly based on laboratory modelling; there is a lack of published information on the actual scour and sedimentation behaviour of pipelines in the field to compare against those results. Bruschi et al. (1997) discussed pipeline self-burial in the field, while Pinna et al. (2003) provided detailed observations for a particular pipeline. More recently Leckie et al. (2015) and Leckie et al. (2016a) have presented detailed analysis of sediment mobility-induced changes to pipeline embedment and spanning for pipelines offshore Western Australia (WA).

Following on from the work of Leckie (2015, 2016a), this paper uses 11 years of field survey data to quantify changes in pipeline embedment and the associated changes in on-bottom stability due to sediment mobility for a pipeline offshore WA. A brief overview of the pipeline

setting and the post-lay near-pipeline bathymetry is presented first, with an emphasis on the aspects of the geometry that have the greatest influence on pipeline stability. The evolution of the on-bottom stability of the pipeline is then considered under the action of a uniform perpendicular current. Finally, the sensitivity of pipeline stability to the pipeline specific gravity (S.G.) is examined to explore the implications of seabed mobility for pipeline design practice.

2 PIPELINE SETTING AND SURVEY DATA

The first 6.5 years of sediment mobility-induced changes to the embedment and spanning of the pipeline considered herein are discussed in detail in Leckie et al. (2015) along with details of the pipeline structural properties and the geotechnical and metocean setting. In summary, the pipeline is 22.9 km long, has a nominal diameter of 12 in. (0.30 m) and was laid in 2001 offshore WA (see Leckie et al. 2015). The seabed soils are relatively uniform along the pipeline route, comprising carbonate sandy SILT (typical d_{50}=0.07 mm) through the middle Kilometre Point (KP) range and carbonate silty SAND (typical d_{50}=0.12 mm) at the two ends. The pipeline lies in 130 m of water depth, which is sufficiently deep that wave induced orbital velocities are negligible at this location. Rather, sediment transport is controlled by tide and internal wave-induced currents which flow perpendicular to the pipeline orientation. Current records from a nearby platform and results from erosion testing indicate that the seabed adjacent to the pipeline is mobile, on average, 7% of the time (a cumulative 25.6 days/year), while the whole seabed is mobile 0.04% of the time (a cumulative 3.5 hours/year) (see Leckie et al. 2015).

Leckie et al. (2015) used annual survey data dating back to 2002, including (i) observations of span start and stop points from pipeline inspection video, and (ii) near pipeline bathymetry for three 200 m sections, which was extracted from historic two-source sonar footage using an image analysis technique described in Leckie et al. (2016b). The first 19 km of the same pipeline was surveyed again in 2013 using more modern multibeam bathymetry and the results made available to the authors after the publication of Leckie et al. (2015).

This 2013 bathymetry forms the basis of the work described in this paper, supplemented with comparisons to the earlier 200 m subsection datasets presented in Leckie et al. (2015). The 2013 multibeam dataset consists of a grid of points either side of the pipeline with a resolution of ~0.2 m centres. While the raw multibeam data is of high quality, post-processing of the data has been undertaken to remove occasional errors and artefacts from the dataset and to interpolate the level of the seabed through the sonar shadow section that exists beneath spanning

sections of pipeline. The raw data, which was referenced to an absolute level, has been transformed to relative level bathymetry with the bottom of the pipeline acting as the reference point (see Figure 2). To assist with computational time, the 0.2 m grid has been interpolated to a grid that has a curvilinear coordinate following the pipeline (with 0.1 m grid spacing) and a second coordinate normal to the pipeline (with 0.1 m grid spacing up to a distance 5 m either side of the pipeline centre). An example of the post-processed bathymetry is shown in Figure 3.

Due to the difficulties in accurately interpolating the depth of shallow spans from multibeam data, visual confirmation from ROV video of the locations where spans start and stop remains the most accurate measure of these points, and has been used herein. While the post-processing produces good quality bathymetry through the sonar shadow region, the depths of very shallow spans (< ~0.25D) should only be taken as indicative.

3 NEAR PIPELINE BATHYMETRY

3.1 Overview

Leckie et al. (2015) provide an overview of the post-lay changes in near-pipe seabed level that occurred between the laying of the pipeline in late 2001 through to 2008. At the time of the most recent survey in 2013, 40 % of the pipeline was in span; a slight increase from the 2008 value of 38%, but within the ‘mature’ range described in Leckie et al. (2015). The mean number of spans per kilometre had reduced slightly from 36 in 2008 to 30 in 2013. Taken together these figures suggest that between 2008 and 2013 the pipeline remained in the ‘pseudo-static’ embedment state described in Leckie et al. (2015), albeit with a slight increase in the number of longer spans.

The free span screening length for vortex-induced vibrations (VIV) on this pipeline is 24 m. Of the 27 such spans that were observed in the annual surveys from 2004 to 2008 and in 2013, only 4 were observed in consecutive surveys. None were observed in 3 or more consecutive surveys. While of only minor importance in the context of on-bottom stability, the transient nature of these spans is an important consideration when considering their integrity and in particular the merits of pipeline intervention works to address concerns surrounding VIV (Krawczyk et al. (2013).

An overlay of the spanning and embedded cross-sections for three 200 m long sections of

pipeline is shown in Figure 4, together with an indication of the percentage of pipeline length in span and embedded. Both the embedded and spanning sections of pipeline are similar for all three sections of pipeline in 2002, in that the embedded sections display high local embedment and relatively low mid and far-field embedment (see Figure 2 for definitions) and the majority of the scour holes are shallow through the spanning lengths of pipeline. By 2006 the embedment and spanning patterns for each of the three sections had changed, but the changes in the sections KP 7.2 – 7.4 and KP 13.3 – 13.5 are the most striking. Here the local, mid- and far-field embedment have increased through the embedded sections (consistent with the idea that the pipeline has sunk into the seabed at supporting shoulders between spans), and the span profiles have both deepened and widened. Between 2006 and 2013 the spanning sections do not change significantly, but the embedment of the embedded sections has continued to increase. Slightly higher seabed levels are present on the starboard (onshore) side in each survey, particularly in 2006 and 2013. For pipeline section KP 19.9 – 20.1 there is little increase in embedment between 2002 to 2006, as might be expected if the pipeline has mainly lowered via sagging at localised (and relatively widely spaced) scour holes.

On the basis of the embedment and spanning patterns along the pipeline from 2002 to 2008, Leckie et al. (2015) established two distinct zones along the pipeline: Zone A covers the two ends of the pipeline and Zone B covers the mid-section from KP ~5 to KP ~16. Approximate values state that there is a transition between the two zones. By 2008 (the final survey considered in Leckie et al. (2015)) Zone A was characterised by a relatively low degree of spanning, moderate to high local embedment and low mid-field embedment, while Zone B was characterised by a high percentage of pipeline in span, and moderate to high local and relatively uniform high mid-field embedment. The Zone A characteristics are indicative of a pipeline that has sagged locally into widely space scour holes, while those for Zone B are indicative of a pipeline that had sunk uniformly into the shoulders between closely spaced scour holes. As indicated in Figure 14, by the time of the 2013 survey, the spanning pattern remained largely unchanged compared to the 2008 values.

The 2013 survey was the first time that the embedment was measured along the full length of the pipeline; the local and mid-field embedments are summarised in Figure 5 and discussed further in Section 3.2.

3.2 Cross-sectional geometry of embedded sections

Considering now the embedded sections of pipeline in isolation, Figure 5 shows 5^{th}, 50^{th}, and

95th percentiles of local and mid-field embedment along the pipeline in 2013 compared to their estimated values immediately after lay in 2001. These statistics have been collected within a 1 km long window which has been shifted along the pipeline in 500 m steps. In addition to highlighting the significant increase in embedment due to sediment mobility over time, the figure demonstrates that on mobile seabeds the seabed is often not flat perpendicular to the pipeline due to the development of scour holes or sedimentation berms adjacent to the pipeline. This contrasts to the conditions often simulated in model tests of pipe-seabed interaction, in which a pipe is penetrated into a flat seabed to investigate the resulting lateral resistance - see Verley and Sotberg (1994) for instance.

The embedment variation is explored further in Figure 6, where the relationship between the local-field embedment and the slope between the local-field embedment and the mid-field embedment level is plotted for the three subsections mentioned earlier. The data fit a straight line relationship; high local-field embedment is associated with negative slopes down away from the pipeline, and low local-field embedment is associated with positive slopes up away from the pipeline. The influence of this type of bathymetry on the pipe-seabed resistance has been explored via numerical analysis by Tom et al. (2015), and the lateral soil resistance modelling approach detailed therein is applied in the stability model detailed later in Section 4.

3.3 Cross-sectional geometry of spanning sections

An analysis of the maximum scour hole depths from 2002 to 2008 included in Leckie et al. (2015) gave scour hole depths (normalised by pipeline diameter) ranging from near zero to 2.5 *D*. A histogram of the scour hole depth (as defined in Figure 2) of all spanning sections in 2013 (sampled at 1 m centres) is presented in Figure 7. Similar scour hole depths are seen, with depths from 0 to 0.5 *D* being the most common. In terms of on-bottom stability these scour hole depths - or ‘gap heights’ in pipeline stability terminology - afford the pipeline significant reductions in both drag and lift force. For instance, drag and lift forces, respectively, can reduce by more than 40 and 80 % respectively of their zero-gap values for scour depths greater than 0.2 *D* (Aamlid et al., 2010).

A histogram of the scour hole half widths W_1 and W_2, (see definition in Figure 2) in 2013 is presented in Figure 8, with the scour hole edge defined as the point where – moving away from the pipeline centre – the local slope of the seabed reduces to less than $14°$. This definition was arrived at by trial and error via manual examination of various spanning profiles of differing slope uniformity and span geometry. Span widths of around 5 ± 0.5 *D* are the most common,

but are distributed about this mean on both sides of the pipeline and range from 2 *D* to 10 *D*.

With respect to Figure 8 it is important to note that the design code DNV-RP-F105 (termed F105 hereafter, Det Norske Veritas (2017)), which is used for the integrity analysis of free spanning sections of pipelines (and is used herein for the calculation of forces on spanning sections; see Section 4.1 for further details) uses the seabed height at a distance of 3.5 D from the centre of the pipeline to estimate the sheltering effect of scour holes (or 'trenches' in the wording used in F105). However, as shown in Figure 8 (and Figure 4) scour holes can be wider than 3.5 *D*. To understand what effect this underestimation of the scour hole width may have, Figure 9 presents a histogram of the difference between the seabed level at an offset distance of 3.5 *D* and the level at the edge of the span coinciding with the definition of the half widths W_1 and W_2 described above. There is a significant difference in the elevation, which means that F105 may underestimate the degree of sheltering, however, additional numerical or physical modelling would need to be carried out to fully understand the effects of the changed geometry. These effects may have implications for a stability analysis that uses the force correction factors given in F105 and, perhaps more importantly, the analysis of pipeline integrity accounting for VIV.

4 ESTIMATED CHANGES IN ON-BOTTOM STABILITY

4.1 Modelling approach

4.1.1 Overview

As a result of the varying pipeline embedment and spanning conditions described above, the lateral on-bottom stability of the pipeline is expected to vary along its length and through time. To estimate these changes a stability analysis is undertaken in this section using (i) the local seabed bathymetry observed in the field; (ii) the pipeline structural properties, (iii) hydrodynamic loads from the industry recommended practices F105 and DNV-RP-F109 (termed F109 hereafter, Det Norske Veritas (2017)), (iv) a pipeline lateral resistance model based on that described in Tom et al. (2015) to estimate the pipe-seabed resistance (see Equation (3) below), and (v) a beam bending analysis to account for vertical and horizontal load sharing along the pipeline between spanning and embedded section of pipe. Each of these aspects of the analysis approach are outlined in Figure 10 and described in more detail below, whilst the beam bending model is shown in schematic form in Figure 11. The pipeline stability is assessed using the criteria of 'absolute stability - virtually stable' described in F109, where the pipeline is considered stable provided displacements do not exceed half the diameter of the

pipeline at any location. The design hydrodynamic loading condition considered in this paper is a uniform perpendicular steady current (attacking the pipe from either direction). This loading condition has been chosen for simplicity and to allow for an uncomplicated assessment of relative changes to the stability of the pipeline. At shallower water sites the combination of waves and currents would need to be considered.

4.1.2 Querying of bathymetry

In the first step, the bathymetry dataset is queried to determine the scour depth S (i.e. gap) as well as the local-field embedment e_l and the mid-field embedment e_m either side of the pipeline (as defined in Figure 2) at one metre centres (or nodes) along the pipeline length. Spanning sections are then separated from embedded sections based on the elevation of the seabed along the pipe centreline (i.e. spans are defined when $S > 0$ at a given node).

The local embedments are then split into subsets based on the chosen direction of the loading. For spanning sections, this leads to the definition of the 'upstream' local embedment e_{lu} and mid-field embedment e_{mu}. For embedded sections of pipeline both the upstream and downstream embedments are of relevance, and are defined for the local embedment (e_{lu} and e_{ld}) and mid-field embedment (e_{mu} and e_{md}) along with the slope (relative to horizontal) of a straight line connecting the mid and local field seabed level on the downstream side of the pipeline (θ_d).

4.1.3 Calculation of load

Together with information on the flow conditions, the embedments and scour depth are used to calculate the horizontal and vertical loads normal to the pipeline at each node. In steady flow conditions (which are assumed in this paper), these loads reduce to the following form for both embedded and spanning sections of pipeline;

$$F = \psi . \frac{1}{2} . \rho_w . D . C . U^2 \quad (1)$$

where F is the force (either the horizontal force F_Y, or the vertical lift force F_Z), ψ is a load correction factor, ρ_w is the density of seawater (taken as 1025 kg/m^3), D is the pipeline diameter (0.3509 m in this case), C is the load coefficient (C_Y or C_Z) and U is the perpendicular component of the steady flow velocity averaged over the height of the pipe (for the purely horizontal flow condition considered herein). The load correction factors (denoted by r and termed reduction factors in F109, or denoted by ψ and termed correction factors in F105 and

herein) account for the influence of the particular flow conditions and the shielding provided by the specific seabed geometry at each node (i.e. $\psi(S, e_{lu}, e_{mu})$; see Figure 10). Note the z_p term of F109 is referred to as e_{lu} herein.

For spanning sections of pipeline, F105 is used to estimate the load coefficients and correction factors for horizontal loads (also known as in-line and lateral loads) on the spanning sections (via Section 5.4 in F105). Alternatively, for the lift forces on spanning sections of pipeline F109 is used for the load coefficient, whilst the correction factor is taken from Figure A11 of DNV '81 (see Aamlid et al. (2010)) as a function of the gap beneath the pipeline (i.e. S herein). Estimating the loads for spanning sections of pipe using these methods ensures that the forces on spanning sections of the pipeline make some allowance for;

- The proximity of the seabed beneath the section of pipe.
- The sheltering provided by the embedment in the mid-field, termed a 'trench' effect.

Due to the short span lengths that occur along this pipeline, corrections for the lateral drag amplification caused by cross-flow vibrations have not been made when using F105.

For embedded sections of pipeline the lateral and lift forces are calculated using F109 (specifically Section 3.6.4 in F109) using the upstream local embedment to define the penetration depth. In this way corrections (only reductions) to the load are made for:

- The permeability of the seabed.
- The sheltering provided by the local embedment, termed 'penetration'.
- The sheltering provided by the mid-field embedment, termed 'trenching'.

Because the goal of this work is to examine the evolution of the pipeline stability as the seabed conditions change, safety factors are not applied to the loads and resistances. Also, we have not explored the influence of modifications to the code-defined approaches, even where recent research suggests modifications may be justified. For instance, a 0.7 reduction in lift force due to a permeable seabed was applied for consistency with the F109 stability approach, although recent work by An et al. (2011) suggests this correction factor may not be justified. This approach has been taken as the focus herein is on the *relative* stability of the pipeline incorporating the effects of sediment mobility.

Finally, as mentioned above the span lengths considered herein were relatively short (with length to diameter ratios generally less than 30) and occur in areas of high stability. As a result, calculation of any amplification of the inline drag force on a spanning section of pipeline due

to cross-flow VIV has not been included. However, on projects where longer spans might occur the influence of this effect would need to be considered in design as the resulting correction factors on the loading are considerable, ranging from 1 to 2.55. However, the dominating design concern would be VIV for such cases.

4.1.4 Vertical beam bending

With the loads calculated, the resulting non-uniform vertical load is then applied and the beam bending equation solved vertically to provide the soil reaction force (F_C) along the pipeline length. A finite difference method is used to solve the beam bending equation, given by;

$$EI\frac{d^4z}{dx^4} - T\frac{d^2z}{dx^2} = W' - F_Z(x) - k(x)z(x), \quad (2)$$

where EI is the pipeline bending stiffness, T is tension in the pipe, x is position along the pipe, $z(x)$ is the vertical displacement of the pipe, W' is the pipeline self-weight, $F_Z(x)$ is the vertical lift force per unit length along the pipe and $k(x)$ is the vertical soil stiffness, which is zero at spanning sections of pipeline and is calculated as described in Leckie et al. (2015) for embedded sections of pipeline with $k(x) = \frac{k_{qc}B}{\lambda}$ where k_{qc} is the gradient of the CPT tip resistance (k_{qc}) with depth in the top metre of seabed, λ is a scaling parameter, to link between the cone and pipe penetration responses (taken as 10) and B is the contact width between the soil and pipeline given by $B = 2D\sqrt{\frac{e}{D} - \left(\frac{e}{D}\right)^2}\ if\ e < D/2$. The vertical soil reaction force is given by $F_C(x) = k(x)z(x)$.

4.1.5 Available soil resistance

Following evaluation of the soil reaction force the available soil resistance to lateral movement is then calculated. A horizontal resistance model is described in DNV-RP-F109, which, in the case of sandy soils, is based on physical model tests described in Verley and Sotberg (1994). However, as described in Tom et al. (2015) and discussed earlier in Section 3.2, those tests do not cover the wide range of local and mid-field embedments encountered on mobile seabeds. To overcome these shortcomings, the approach described in Tom et al. (2015) is applied herein. More specifically, the maximum available horizontal resistance is calculated such that;

$$\frac{F_r(x)}{F_C(x)} = c_\theta \mu_{brk,\theta=0}, \quad (3)$$

where $F_r(x)$ is the available horizontal soil resistance, $F_c(x)$ is the vertical pipeline contact

force (obtained from the solution of equation (2)), $\mu_{brk,\theta=0}$ is the lateral friction coefficient assuming a flat seabed and c_θ is a correction factor that accounts for the effect of a sloping seabed adjacent to the pipeline. The ratio F_r/F_c is termed the 'friction factor'.

To evaluate equation (3), firstly $\mu_{brk,\theta=0}$ is interpolated from numerical limit analysis results reported in Tom et al. (2015) (see Figure 14 of that paper). Those results are means of upper and lower bound results assuming associated flow, a friction angle of 30°, and a flat seabed. The resulting ratios are shown on Figure 12, with the values assumed herein for local embedments outside the range considered in Tom et al. (2015) indicated by dashed lines.

Secondly, the correction factor c_θ is applied to account for the effect of the seabed slope between the local and the mid-field embedment (this angle θ is defined on Figure 6). The results of Tom et al. (2015) are used again. They used further numerical modelling to establish a relationship for 'friction up a hill' (where the slope angle is added (or subtracted) from the soil friction angle). The resulting correction factor c_θ is plotted for a range of slope angles on Figure 12.

This is a relatively simple approach to the modelling of pipe-soil interaction forces, consistent with the simplified form of loading that is considered, and consistent with codified stability design methods. More detailed soil models have been proposed to capture undrained conditions, the interaction between vertical load and friction coefficient, and the gross deformation of the seabed by 'bulldozing' effects (e.g. Randolph & White (2008), Tian & Cassidy (2008) and White & Cheuk (2008)). However, the purpose of the present analysis is to assess the relative changes in stability due to changes in embedment, and it is anticipated that this relative stability would be broadly independent of the adopted soil model.

4.1.6 Horizontal beam bending

With the loads and resistances calculated, the beam bending equation is then solved horizontally to calculate the lateral displacement for a given applied horizontal velocity. In this calculation the beam bending equation is given by;

$$EI\frac{d^4y}{dx^4} - T\frac{d^2y}{dx^2} = F_Y(x) - F_r'(x), \qquad (4)$$

where y is the lateral displacement of the pipeline, $F_Y(x)$ is the horizontal (or lateral) hydrodynamic force and $F_r'(x)$ is the mobilised horizontal soil resistance. At locations where the pipeline is embedded the load displacement relationship is modelled as elastic-perfectly

plastic (see inset to Figure 11) with the soil resistance given by;

$$F_r'(x) = \begin{cases} F_r(x)\dfrac{y}{y_{mob}}, & y \le y_{mob} \\ F_r(x), & y > y_{mob} \end{cases}, \quad (5)$$

where y_{mob} is the mobilisation distance (set equal to $0.1D$). This mobilisation distance value lies between the results of Verley and Sotberg (1994) and Zhang et al. (2002). The sensitivity of the analysis to the mobilisation distance has been analysed across a range of 0.05 D to 0.2 D, with the resulting critical velocity only varying by 0.02 m/s within this range. The pipeline was equidistantly discretised with the finite difference approach. The sensitivity to the size of the discretisation was analysed and a satisfactory convergence was achieved for elements of 1.0 m of length.

Solution of Equation (4) allows for accommodation of the 'smearing' or load-sharing effect that the pipeline bending stiffness has on the loads and soil resistance. Zero moment and displacement end conditions are assumed as boundary conditions in the solution, and a 200 m buffer either side of the 200 m section of pipeline under consideration is used to ensure that the boundary conditions do not influence the displacement solution through the analysis section.

The critical velocity is found, when the horizontal displacement of the pipeline exceeds 0.5 D at any point along the central 200 m.

4.2 Quasi 2D Analysis

It should be noted that the beam bending approach outlined in Section 4.1 assumes that the hydrodynamic forces and lateral soil 'friction factor' may be estimated based on the local 2D geometry at each node along the pipeline. The interaction between successive nodes is then accounted for by the beam bending model. This type of quasi-2D analysis approach is used commonly by industry (with varying levels of sophistication), however, it should be noted that there is a lack of conclusive analysis to indicate whether or not it is valid to treat the hydrodynamic force as the aggregation of forces based on 2D cross-sections (see Griffiths et al. (2012), Shen et al. (2013)), and to treat the local friction factors as locally 2D (i.e. based on the assumption the pipeline is translating perpendicular to its length only). To properly assess the quasi-2D analysis approach, 3D analysis would be of benefit in future work (providing computational requirements are not prohibitive). Nevertheless, it is expected that general conclusions concerning relative changes in stability will be consistent regardless of the analysis approach, and for this reason the quasi-2D approach is adopted in this paper.

4.3 Results

4.3.1 Load and resistance variation due to sediment mobility

An example output from the model subjected to a 1 m/s current (mean velocity across the pipeline diameter) is shown for a 200 m section of pipeline in Figure 13. This represents a strong, but not untypical loading for offshore WA; for example Van Gastel et al. (2009) report currents of ~1 m/s associated with internal waves, while Leckie et al. (2016a) report values of up to 2 m/s possibly associated with breaking internal waves. The figure outlines, from top to bottom; (i) the locations of spans, (ii) the seabed level in the local-field and mid-field, (iii) the load distribution along the pipeline, (iv) the vertical contact force and available lateral resistance distribution along the pipeline, and (v) the lateral displacement of the pipeline. The values for these parameters for the as-laid embedment condition are indicated by dashed lines, whilst for the 2013 condition they are indicated by solid lines.

Comparisons of these lines show how the lateral (F_Y) and lift (F_Z) forces both reduce from the as-laid condition, with lift reducing by around 70% along the majority of the embedded lengths of pipeline and almost to zero over the majority of the spanning lengths. As a result of this lift reduction and the formation of pipeline spans, the vertical contact force (F_c) between the pipeline and the seabed increases by 2013, with particularly high values apparent at the span shoulders where the soil supports the additional pipeline weight from the spans. The increase in contact force, coupled with the significant increases in local and mid-field embedment, leads to an increase in the available resistance to lateral movement (F_r) at embedded sections. Inspection of the F_c and F_r profiles shows that the 2013 'friction factors' exceed unity for almost all of the embedded length of pipeline. The reduction in loading coupled with the increase in available resistance results in a large increase in pipeline stability. The maximum lateral deflection for the 2013 condition is only 22% of the deflection under the as-laid condition.

4.3.2 Stability variation along the pipeline

By iterating on the velocity magnitude, the model has been used to determine the 'critical' steady current velocity (U_{crit}) for which a given section of pipeline will 'break out' or displace laterally by 0.5 *D*. The critical velocity along the pipeline is shown in Figure 14. To prepare this figure the critical velocity has been computed separately for successive 200 m sections of the pipeline, both for an offshore current and an onshore current. For the offshore loading case average values within each 200 m section are shown for the applied lateral and lift loads, the

vertical contact force, and the available soil resistance. While these average values of the load and resistance do not rigorously account for load and resistance sharing along the pipeline in the way that the model does, they indicate the general trend along the pipeline. Statistics on the spanning state of the pipeline are also shown.

The critical velocity for the as-laid condition is also shown, along with the loads, contact force and available resistance when the critical velocity for the 2013 condition for each particular 200 m section is applied to the as-laid condition. When the 2013 critical velocity is applied to the as-laid pipeline-seabed geometry, the lateral and lift forces range from ~0.75 to ~1.5 kN/m. This lift force is sufficiently high to lift sections of pipeline off the seabed, resulting in zero available resistance and the failure of the pipeline under the absolute stability criterion.

In contrast, when the same load is applied to the pipeline with the 2013 embedment condition, lift loading is reduced to <0.25 kN/m and the lateral force to <0.69 kN/m. The reduction in lift load ensures that a positive vertical contact force is maintained along the pipeline, thus enabling a lateral resistance ranging from 0.21 to 0.79 kN/m. These changes result in a 1-2 m/s increase in the critical velocity by 2013 compared with the as-laid value of 1.07 m/s. There is a minor variation in the offshore and onshore values of critical velocity due to asymmetric seabed levels either side of the pipeline, with the offshore direction giving the lower critical velocity, typically.

The critical velocity varies along the pipeline (Figure 14). The higher critical velocity through the mid-section of the pipeline (relative to the two end sections) is accompanied by an increase in the available resistance to lateral movement. Inspection of the embedment variation (see Figure 5) shows that the resistance increase through the central sections is in turn due to increases in both the local and the mid-field embedment through this zone (with the higher mid-field embedment attributable to the fact that the pipeline has lowered relatively uniformly due to scour in this section; see Leckie et al. (2015)).

Plots of the percentage of pipeline in span (*Span*) and the average ratio of the added half-lengths of the embedded sections of pipeline either side of a span to the length of that span (L_{embed}/L_{span}), are included in Figure 14. The values shown are averages of these parameters for each 200 m analysis section. While the percentage of pipeline in span increases through the mid-section of the pipeline, there is significant variation within this overall trend and this variation is not reflected in the critical velocity profile. This suggests that the span ratio does not have a direct influence on the stability of this particular pipeline. However, the spanning ratio does have an indirect influence, as in this case it is consistent with the uniform lowering of the pipeline mid-

section (Zone B) primarily through pipeline sinking at span shoulders (Leckie et al., 2015), which explains the higher midfield embedment that this section enjoys. Similarly, the L_{embed}/L_{span} ratio tends to be low through the mid-section of the pipeline. While this suggests that this parameter is not critical in terms of mobilising sufficient lateral soil resistance, it does reflect the above-mentioned pipeline lowering history.

4.3.3 The relative influence of hydrodynamic load reduction and increased soil resistance

From inspection of Figure 13, both increases in lateral soil resistance and reductions in lift and horizontal load are evident over the 200 m section of pipeline compared with the as-laid embedment profile. To further explore how the changes in lateral soil resistance and in hydrodynamic load both effect stability, Table 1 presents – for the full pipeline length – the average load and resistance values in both the as-laid and the 2013 condition, for the same 1 m/s perpendicular current shown on Figure 13. It can be seen that the lateral and vertical hydrodynamic force reduce by a factor 2.5 and 6.5, respectively, due to sheltering and spanning in 2015. In comparison the available lateral soil resistance increases by a factor of 3.8. Thus the reduction in hydrodynamic load due to sheltering and the increase in lateral soil resistance make similar contributions to the increased stability in 2013.

Table 1: Hydrodynamic load and soil resistance changes from as-laid to the 2013 condition under 1 m/s steady current.

		As-laid value	2013 value
$\overline{F_Y}$	[kN/m]	0.15	0.06
$\overline{F_Z}$	[kN/m]	0.13	0.02
$\overline{F_C}$	[kN/m]	0.33	0.44
W'	[kN/m]	0.46	0.46
$\bar{F}_r$	[kN/m]	0.18	0.69
$\bar{F}_r/\bar{F}_c$	[ ]	0.55	1.6
$\overline{F_r'}/\bar{F}_r$	[ ]	0.83	0.08

Note: Values with overbars are averaged over the length of the pipeline.

Each of the values listed in Table 1 will vary with the applied current velocity. The sensitivity of these parameters to the current velocity is explored in Figure 15, which shows the failure lines (i.e. the friction limits indicating the maximum available lateral resistance for a given vertical contact force) and load paths (i.e. the lateral and vertical force, net of weight, for different current velocities) for the as-laid and 2013 condition. For the 2013 condition case, the values presented are averages for the entire pipeline length. The as-laid conditions are assumed

to be uniform.

The failure lines indicated by the friction limits on Figure 15 highlight the significant increase in soil resistance between the as-laid to the 2013 condition; for a given vertical contact force (F_c), almost three times the horizontal resistance can be mobilised in 2013. The differing load paths and the coordinates of points of a given velocity highlight how the loading has also changed in two significant ways due to seabed mobility; (i) the magnitude of both lift and horizontal (or drag) force has reduced in the 2013 condition for any given applied current velocity, and (ii) the ratio of drag to lift has increased, which allows for fuller utilisation of the bottom right hand corner of the failure envelope. This is advantageous for the pipeline stability; had the ratio of drag to lift been maintained between the as-laid and 2013 condition, the load path would have crossed the failure line at a lower value of F_c, and at a lower current velocity, reducing the gain in stability. Hence for the conditions considered herein, Figure 15 further demonstrates that both hydrodynamic load reduction (through sheltering) and increased soil resistance contribute to the increase in stability.

In light of the observations in Table 1 and Figure 15, it is interesting to consider if certain situations may arise in which it is possible to separate the relative influences of a reduction in hydrodynamic load and an increase in lateral soil resistance on stability and, in turn, to determine if either effect was more dominant. We can explore this question by noting that a pipeline will become unstable on a flat seabed when;

$$\rho_w C_Y D U^2 > \mu(2W' - \rho C_Z D U^2) \tag{6}$$

Rearranging (6) gives the following at the point of instability;

$$U_{crit} = \sqrt{\frac{2W'}{\rho_w D}\left(\frac{\mu}{C_Y + \mu C_Z}\right)}. \tag{7}$$

The values affected by embedment are inside the brackets and control the relative importance of drag, lift and soil resistance. As μ increases, lift becomes increasingly important, and in the limit as $\mu \to \infty$ (7) reduces to;

$$U_{crit} = \sqrt{\frac{2W'}{\rho_w D C_Z}}, \tag{8}$$

and the pipe can only be destabilised by being lifted off the seabed, rather than sliding across it. Hence, we can conclude that in this limiting condition, changes in hydrodynamic load (specifically the lift coefficient) would be of most relevance for stability of a pipeline, with a

fractional increase in U_{crit} being equal to the square root of a fractional decrease in C_Z. In contrast, as μ decreases to zero, the drag term dominates in the denominator so (7) reduces to;

$$U_{crit} = \sqrt{\frac{2W'\mu}{\rho_w D C_Y}}, \quad (9)$$

and the pipe will become unstable by sliding across the seabed. In this limiting condition it is, therefore, possible to separate the relative contributions of drag force and resistance on stability and, in turn, to ascertain which effect contributes most to a change in U_{crit}.

For the more general situation in which neither of these limits in μ holds, it follows that drag, lift and soil resistance are all important in determining the pipeline's stability. More importantly, because μ appears in the denominator in (7) the relative influence of changes in the hydrodynamic load and soil resistance cannot be separated; with both effects contributing interdependently to the critical velocity. This situation is most relevant for the present pipeline.

4.3.4 The influence of pipeline specific gravity

In on-bottom stability design the principal objective is to determine the minimum pipeline specific gravity at which the pipeline remains stable in a design storm. The stability analysis presented in Section 4.3.2 was repeated for different values of the specific gravity of the pipeline; all other parameters were kept constant. The results are summarised in Figure 16. Values are shown for the as-laid case, along with the maximum and minimum velocities in each flow direction in 2013. Above the real pipeline S.G. of 1.48, the critical velocity increases in a relatively linear fashion with S.G., while below that value the critical velocity declines non-linearly towards zero at an S.G. of 1.

Figure 16 shows a remarkable difference in required pipeline S.G. for the as-laid and 2013 conditions for a given design current. For example, the real pipeline is stable up to a current of 1.1 m/s in the as-laid condition. However, if the changes in embedment from seabed mobility could be relied upon prior to this flow occuring, then a pipeline S.G. of only 1.1 is required to be stable in the same current. This is significantly lower than the actual S.G. of 1.48 and illustrates the practical benefit of seabed mobility on pipeline stability design – a major reduction in the required pipeline self-weight occurs if seabed mobility effects can be accounted for in the stability design.

These conclusions rest on the assumption that the scour and sedimentation changes around the pipeline are relatively independent of the pipeline S.G. However, consideration of the three main mechanims that are believed to account for the embedment change on mobile seabeds

suggests that this assumption may not be overly limiting. These three mechanisms are (i) direct sedimentation as described in Leckie et al. (2016a) (ii) sagging into long spans and (iii) pipeline sinking at span shoulders (sagging and sinking are both described in Sumer and Fredsøe (2002)). With respect to the first of these mechanisms, namely direct sedimentation, it is expected that this is independent of pipeline S.G (down to an S.G. at which the pipeline is no longer stable under the flow conditions which lead to sedimentation). For the second mechanism, it is evident from beam bending theory that pipeline sagging is more heavily dependant on span length (to the fourth power of span length) than it is on the pipeline self-weight. Finally, with respect to the third mechanism, Sumer and Fredsøe (1994) found that sinking at span shoulders is "practically uninfluenced" by pipeline self weight, and that the process was governed by the progression of scour at the span shoulders.

Finally it is important to recall that other limit states such as pipeline floation under liquefaction (see Sumer et al. (1999) and Bonjean et al. (2008) for instance) may also impose a lower bound limit on the results displayed in Figure 16.

4.3.5 Stability evolution with time

The change in the embedment, loads, available resistance and critical velocity from 2002 to 2013 are displayed for the sections KP 7.2 – 7.4 and 19.9 – 20.1 in Figure 17. The loads in each case result from a 1 m/s steady current flow velocity. The two sections display a contrasting evolution of stability with time. From 2002 to 2013 the section KP 7.2 – 7.4 (which is typical of the mid-section of the pipeline) becomes progressively more stable due to an increase in the local and mid-field embedment. This is because the embedment change led to a progressive decrease in loading, and lateral soil resistance increased by an even larger magnitude. The critical velocity initially increases only slowly from the as-laid value of 1.07 m/s, but by 2013 has reached a value of 2.90 m/s.

In contrast, the section 19.9 – 20.1 generally had a slightly larger initial increase in local embedment, and a higher degree of spanning in the 6 months following laying in 2002. This resulted in a higher critical velocity in 2002 of 1.35 m/s. However, by 2006 only minor additional increases in the local and mid-field embedment had occurred, and the percentage of the pipeline in span had reduced significantly. These changes resulted in a slight increase in the critical velocity to 1.49 m/s. This section of pipeline was not surveyed in 2013, but based on the sections of Zone A that were surveyed in 2013 it is likely to have undergone an increase in embedment and hence stability since 2006.

These changes are explored further in Figure 18, which for a range of assumed pipeline S.G. values shows the post-lay evolution of critical velocity that occurs for these sections of pipeline and the section KP 13.3 – 13.5. For all three sections, small to moderate increases in stability are noticeable 6 months after lay (in 2002). However, by 2006 the critical velocity has increased by approximately 0.6 m/s for the Zone B pipeline sections KP 7.2 – 7.4 and 13.3 – 13.5 assuming an S.G. of 1.43, or 0.8 m/s assuming an S.G. of 2. Further increases occur between 2006 and 2013, with a total increase in capacity from the as-laid position of 1.7 m/s or 2.4 m/s at the same two S.G. values. Where these changes in embedment could be allowed for in design (through, for instance, a probabilistic considerations of the likelihood of the design storm arriving in the initial years of the pipeline life), the design S.G. for a design current of 1.75 m/s (for example) could be reduced from 2 to 1.16.

In contrast, the section of pipeline from KP 19.9 to 20.1 experienced only a minor increase in stability between 2002 and 2006, no survey data was available for this section in 2013. This later section of pipeline lies within Zone A. The differences between these sections of pipeline and zones are discussed further below.

5 CONCLUDING DISCUSSION

The post-lay changes in spanning and embedment of a pipeline, and the resulting increase in its on-bottom stability, have been reviewed using conventional industry standard approaches to assess pipeline stability for a given embedment state. The 12 in. pipeline is 22.9 km long and laid perpendicular to the tidal and internal wave driven currents that drive sediment transport at the site. The pipeline crosses relatively uniform soils; the two end sections of the pipeline (Zone A) cross silty SAND while the middle section (Zone B) crosses sandy SILT. In the 6 months following lay, spans formed along much of the pipeline length and small increases in the local embedment of the embedded sections occurred. In the next 4 years, the spans deepened, and the average embedment continued to increase in the local and mid-field. Finally, 12 years after lay (in 2013), further embedment increases had occurred, and the spanning pattern was largely stable.

The resulting reductions in pipeline lateral and lift loading – as well as increases in the available soil resistance – led to significant increases in the pipeline stability as assessed using conventional stability design guidelines. For the earlier years detailed bathymetric data has only been analysed for three 200 m long sections of pipeline. Two of those sections (both in Zone

B) evolved at a similar rate, while the third section (in Zone A) showed a more rapid increase in stability over the first 6 months, but then only a small additional increase 4.5 years later, and a lower level of stability at that time relative to the Zone B sections.

By 2006 the post-seabed-mobility profile in Zone B typically consisted of a relatively uniformly lowered pipeline with high local embedment in the embedded sections and high mid-field embedment in both the embedded and spanning sections of pipeline. Such a profile is consistent with pipeline lowering by sinking into span shoulders. In contrast the post-seabed-mobility profile in Zone A consisted of rapid development of increased local field embedment with low mid and far-field embedment in the embedded sections, and high mid- and far-field embedment in the spanning sections. This is consistent with sagging of discrete sections of pipeline coupled with local sedimentation in the intervening embedded sections. These two different modes of pipeline lowering have been shown to result in different rates of stability change, particularly in the early years. But by 2013 the local and mid-field embedment had risen along the entire surveyed length of pipeline.

The resulting stability of the pipeline when subjected to steady current has been assessed via two methods. Firstly the local stability was assessed in the as-laid and 2013 embedment conditions, via a structural analysis of the pipeline allowing for bending and tension. Secondly, the average drag and lift loads and the average soil resistance over the entire length have been compared at the two times. Using both methods it is demonstrated that the stability has been significantly enhanced. The structural modelling showed that in Zone A the critical velocity to cause a lateral pipe movement of 0.5 diameter increased by over 1 m/s, while increases of up to 2 m/s had occurred in Zone B by that stage. The length-averaged analysis showed that the soil resistance had approximately tripled while the lift and drag had reduced by approximately the same factor.

Most fundamentally, the results in this paper highlight the potential value in accounting for sediment mobility effects in design. These effects are time dependent, and will not be available to the pipeline immediately after lay. There are two approaches that may be used to account for this; (i) using probabilistic techniques to determine the likelihood of the design storm occurring before sediment transport under ambient flow conditions has afforded sufficient stability gains to the pipeline, and (ii) considering the ability of the pipeline to adapt to a more stable position in the ramp up period of the design storm. On the first approach Leckie et al. (2015) and Leckie et al. (2016a) provide examples of mobility-driven embedment change under ambient conditions which may be used to validate models in ambient conditions. On the second

approach Draper et al. (2015) have examined experimentally the lowering (and changes to stability) of a pipeline during the storm ramp up period.

While other failure modes (such as buoyant uplift) will set a lower limit to the pipeline design S.G., the significant stability increases highlighted herein demonstrate that accounting for time dependent embedment changes offers significant opportunities for more efficient pipeline stability design.

ACKNOWLEDGEMENTS

This research forms part of the activities of the Centre of Offshore Foundation Systems (COFS), supported as a node of the Australian Research Council's Centre of Excellence for Geotechnical Science and Engineering (CGSE), and through the Fugro Chair in Geotechnics, the Lloyd's Register Foundation Chair and Centre of Excellence in Offshore Foundations, and the Shell EMI Chair in Offshore Engineering, which was held by the third author. The first author acknowledges his Research Studentship support from the University of Western Australia. The first and second authors acknowledge the support of the Lloyd's Register Foundation (LRF). LRF helps to protect life and property by supporting engineering-related education, public engagement and the application of research.

612 **REFERENCES**

613 Aamlid, O., Vedeld, K. and Sollund, H.v., 2010. Effects of free spans on on-bottom stability of
614 offshore pipelines: A global approach. ASME 2010 29th International Conference on
615 Ocean, Offshore and Arctic Engineering, p. 999-1009.
616 An, H., Cheng, L. and Zhao, M., 2011. Numerical simulation of a partially buried pipeline in a
617 permeable seabed subject to combined oscillatory flow and steady current. Ocean
618 Engineering, 38(10): 1225-1236.
619 An, H., Luo, C., Cheng, L. and White, D., 2013. A new facility for studying ocean-structure–
620 seabed interactions: The O-tube. Coastal Engineering, 82(0): 88-101.
621 Bonjean, D., Erbrich, C. and Zhang, G., 2008. Pipeline floatation assessment in liquefiable soil.
622 Offshore Technology Conference, Paper No. OTC 19668, Houston, Texas, USA, 5-8
623 May, 10 p.
624 Bruschi, R., Drago, M., Venturi, M., Jiao, G. and Sotberg, T., 1997. Pipeline reliability across
625 erodible/active seabeds, Offshore Technology Conference.
626 Det Norske Veritas, 2017. Recommended practice DNV-RP-F105, Free spanning pipelines.
627 Det Norske Veritas, 2011. Recommended practice DNV-RP-F109, On-bottom stability design
628 of submarine pipelines
629 Det Norske Veritas, 2017. Recommended practice DNV-RP-F109, On-bottom stability design
630 of submarine pipelines
631 Draper, S., An, H., Cheng, L., White, D.J. and Griffiths, T., 2015. Stability of subsea pipelines
632 during large storms. Philosophical Transactions of the Royal Society of London A:
633 Mathematical, Physical and Engineering Sciences, 373(2033): 20140106.
634 Griffiths, T., Shen, W., Xu, M. and Leggoe, J., 2012. Comparison of recent parametric trenched
635 and partially embedded/spanning pipelines with DNV-RP-F109 load reduction design
636 curves. ASME 2012 31st International Conference on Ocean, Offshore and Arctic
637 Engineering, p. 207-224.
638 Hulsbergen, C.H. and Bijker, R., 1989. Effect of spoilers on submarine pipeline stability.
639 Offshore Technology Conference, Paper No. OTC 6154, Houston, Texas, USA, 1 - 4
640 May, p. 337 - 350.
641 Krawczyk, P., Bijker, R., Chen, Z. and Boersma, H., 2013. Managing free spans on dynamic
642 seabed. Proceedings of OPT-2013.
643 Leckie, S.H.F., Draper, S., White, D.J., Cheng, L. and Fogliani, A., 2015. Lifelong embedment
644 and spanning of a pipeline on a mobile seabed. Coastal Engineering, 95: 130-146.
645 Leckie, S.H.F. et al., 2016a. Sedimentation-induced burial of subsea pipelines: Observations
646 from field data and laboratory experiments. Coastal Engineering, 114: 137-158.
647 Leckie, S.H.F., White, D., Draper, S. and Cheng, L., 2016b. Unlocking the benefits of long term
648 pipeline embedment processes: Image analysis-based processing of historic survey data.
649 Journal of Pipeline Systems Engineering and Practice,10.1061/(ASCE)PS.1949-
650 1204.0000242, 04016008
651 Palmer, A., 1996. A flaw in the conventional approach to stability design of pipelines. Offshore
652 Pipeline Technology Conference (OPT'96), 19th Annual conference, Amsterdam.
653 Pinna, R., Weatherald, A., Grulich, J. and Ronalds, B.F., 2003. Field observations and
654 modelling of the self-burial of a North West Shelf pipeline, ASME Conference
655 Proceedings, p. 591-599.
656 Randolph M.F. & White D.J. 2008. Upper bound yield envelopes for pipelines at shallow
657 embedment in clay, Géotechnique, 58(4):297-301
658 Shen, W., Griffiths, T., Xu, M. and Leggoe, J., 2013. 2D and 3D CFD investigations of seabed
659 shear stresses around subsea pipelines, ASME 2013 32nd International Conference on
660 Ocean, Offshore and Arctic Engineering. American Society of Mechanical Engineers.

661 Sumer, B. and Fredsøe, J., 1994. Self-burial of pipelines at span shoulders. International Journal
662 of Offshore and Polar Engineering.
663 Sumer, B.M. and Fredsøe, J., 2002. The mechanics of scour in the marine environment. World
664 Scientific Publishing, Singapore.
665 Sumer, B.M., Fredsøe, J., Christensen, S. and Lind, M.T., 1999. Sinking/floatation of pipelines
666 and other objects in liquefied soil under waves. Coastal Engineering, 38(2): 53-90.
667 Tian, Y., Cassidy, M.J. 2008, 'Modelling of pipe-soil interaction and its application in numerical
668 simulation', International Journal of Geomechanics, 8, 4, p. 213-229
669 Tom, J.G., Leckie, S.H.F., White, D.J. and Draper, S., 2015. Drained breakout resistance of a
670 pipeline on a mobile seabed, OMAE2015-41206, International Conference on Ocean,
671 Offshore and Arctic Engineering, St. John's, Newfoundland, Canada.
672 Van Gastel, P., Ivey, G.N., Meuleners, M.J., Antenucci, J.P. and Fringer, O., 2009. The
673 variability of the large-amplitude internal wave field on the Australian North West
674 Shelf. Continental Shelf Research, 29(11): 1373-1383.
675 Verley, R.L.P. and Sotberg, T., 1994. A soil resistance model for pipelines placed on sandy
676 soils. Journal of Offshore Mechanics and Arctic Engineering, 116(3): 145-153.
677 White D.J. & Cheuk C.Y. 2008. Modelling the soil resistance on seabed pipelines during large
678 cycles of lateral movement. Marine Structures 21(1):59-79
679 White, D.J. et al., 2014. Ocean-structure-seabed interaction: O-tube modelling of pipeline
680 stability. Australian Geomechanics Journal, 49(4): 157-164.
681 Whitehouse, R.J.S., 1998. Scour at marine structures: A manual for practical applications.
682 Thomas Telford Publication, London, United Kingdom.
683 Zhang, J., Stewart, D.P. and Randolph, M.F., 2002. Modeling of shallowly embedded offshore
684 pipelines in calcareous sand. Journal of Geotechnical and Geoenvironmental
685 Engineering, 128(5): 363-371.
686

Figures

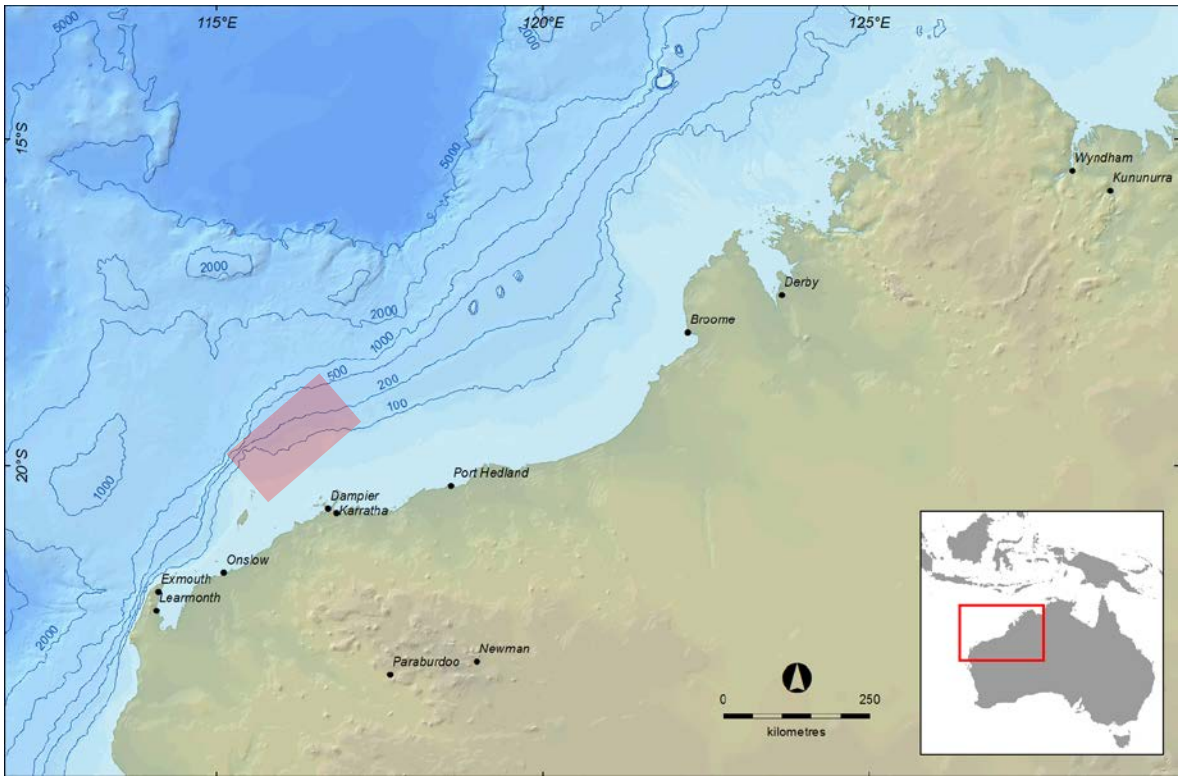

Figure 1: Location of the pipeline and the bathymetry of the North West Shelf. Reprinted from Coastal Engineering, Vol 95, Jan. 2015, S. H. F. Leckie, S. Draper, D. J. White, L. Cheng, and A. Fogliani, "Lifelong embedment and spanning of a pipeline on a mobile seabed," pp. 130–146, Copyright 2014.

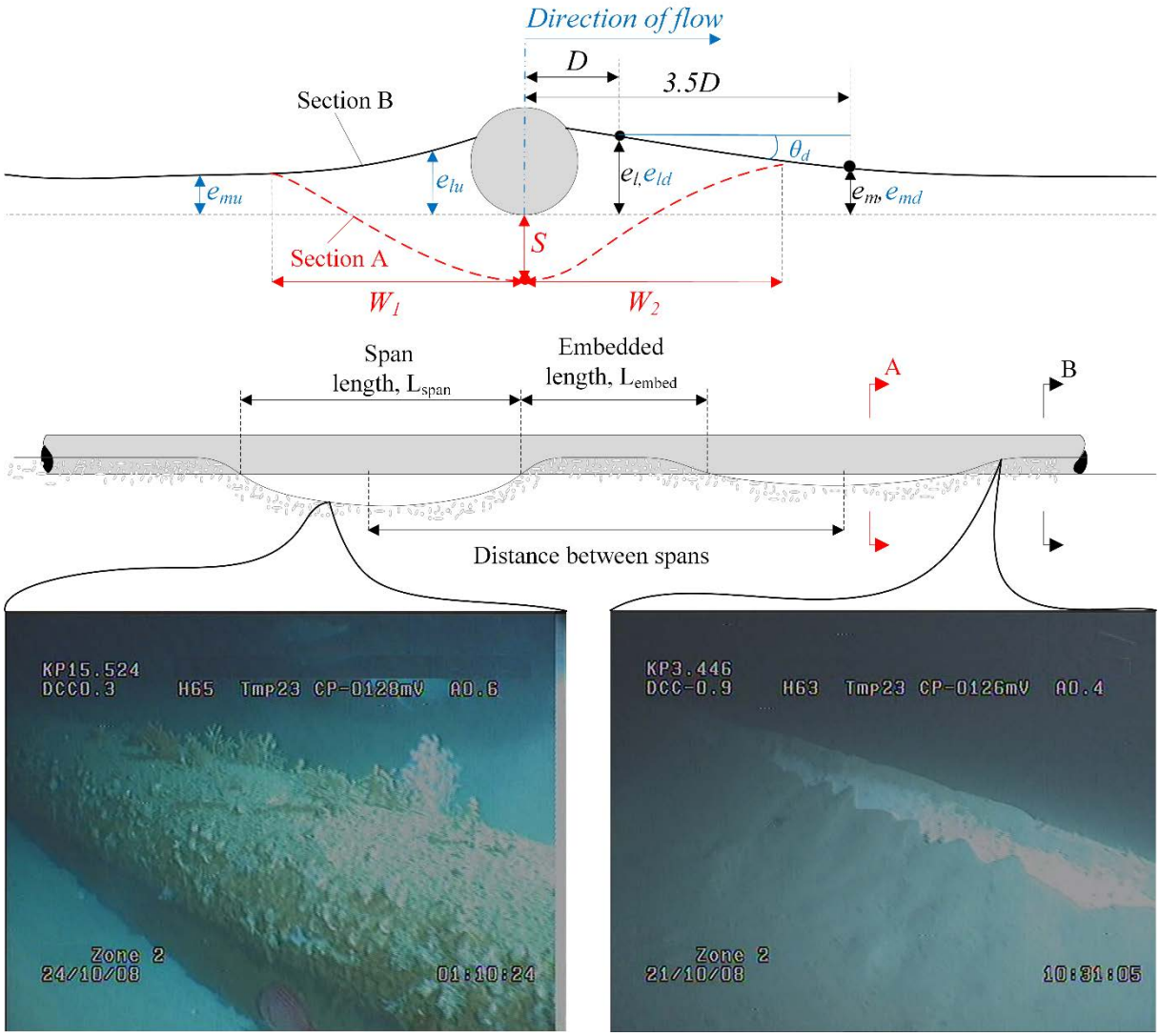

Figure 2: Definition of terms and examples of spanning (left image) and embedded (right image) sections of pipeline; where *D* is diameter, e_l is the local embedment, e_m is the mid-field embedment, *S* is the scour hole depth, W_1 is the port (in this case offshore) scour hole half-width, and W_2 is the starboard (onshore) scour hole half-width, and L_{span} and L_{embed} are as shown. W_1 and W_2 are set at the point where the local slope of the seabed reduces to less than 14 degrees.

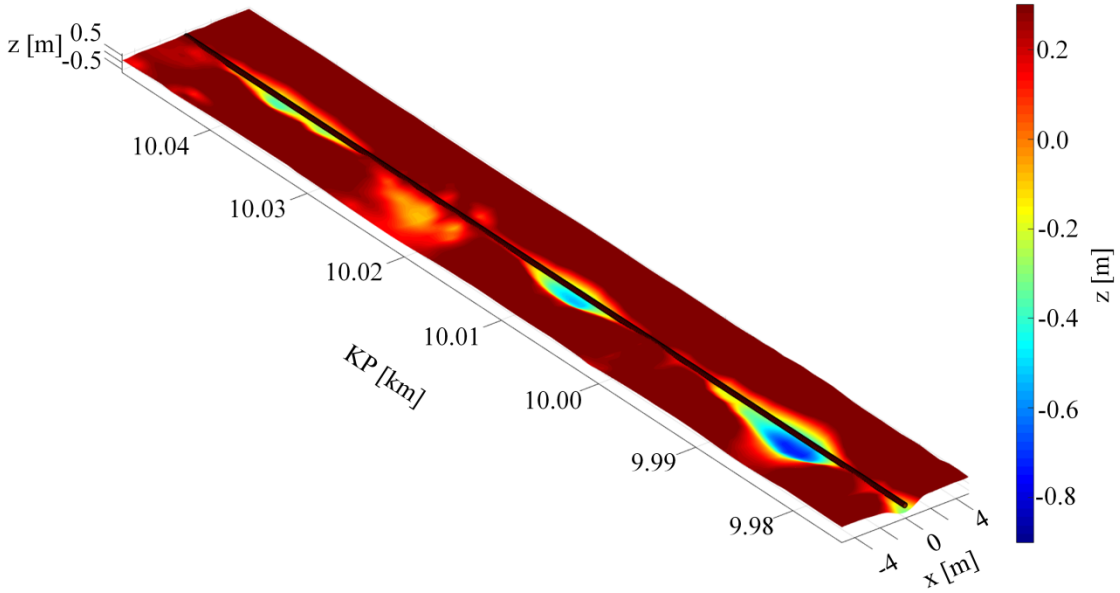

Figure 3: Example of the post-processed 2013 survey bathymetry. Seabed level is shown relative to the bottom of the pipeline.

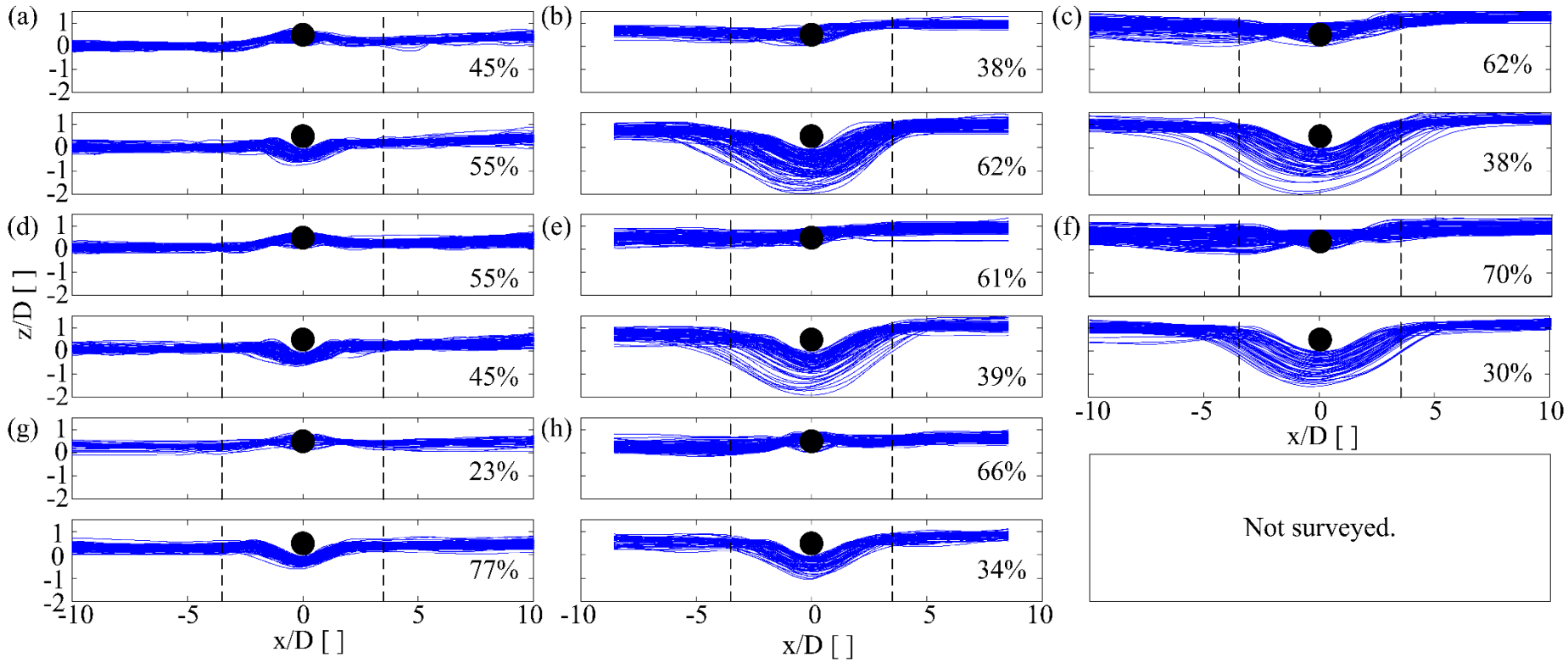

Figure 4: Overlays of spanning and embedded cross-sections for the pipeline sections KP 7.2 – 7.4 in (a) 2002, (b) 2006 and (c) 2013; KP 13.3 – 13.5 in (d) 2002, € 2006 and (f) 2013; and 19.9 – 20.1 in (g) 2002 and (h) 2006. Vertical dashed lines are at 3.5*D* offsets from the pipe centreline. One section is drawn at every meter along the pipeline. The top and bottom plot in each subfigure represent, respectively, the embedded and spanning sections of the pipeline.

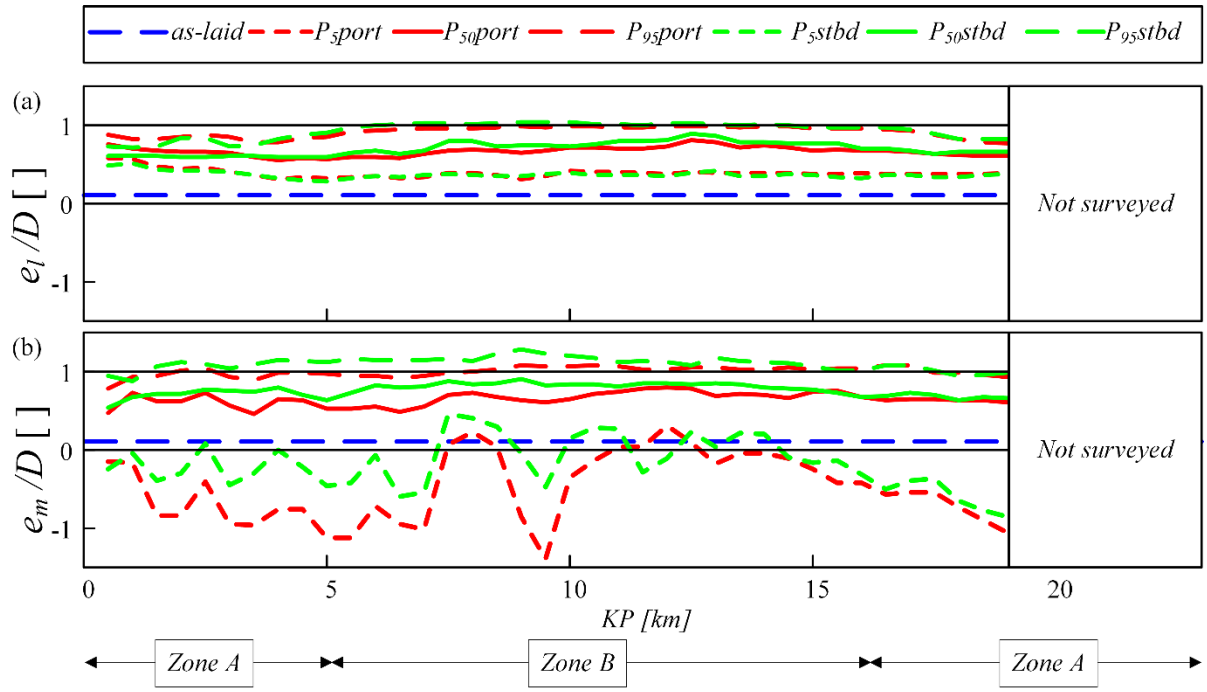

Figure 5: Embedment variation along the pipeline both (a) local to the pipeline and (b) in the mid-field. As-laid variation embedment estimate is shown along with statistics on the 2013 embedment either side of the pipeline, collected within a 1 km long window which is moved in 500 m steps along the pipeline.

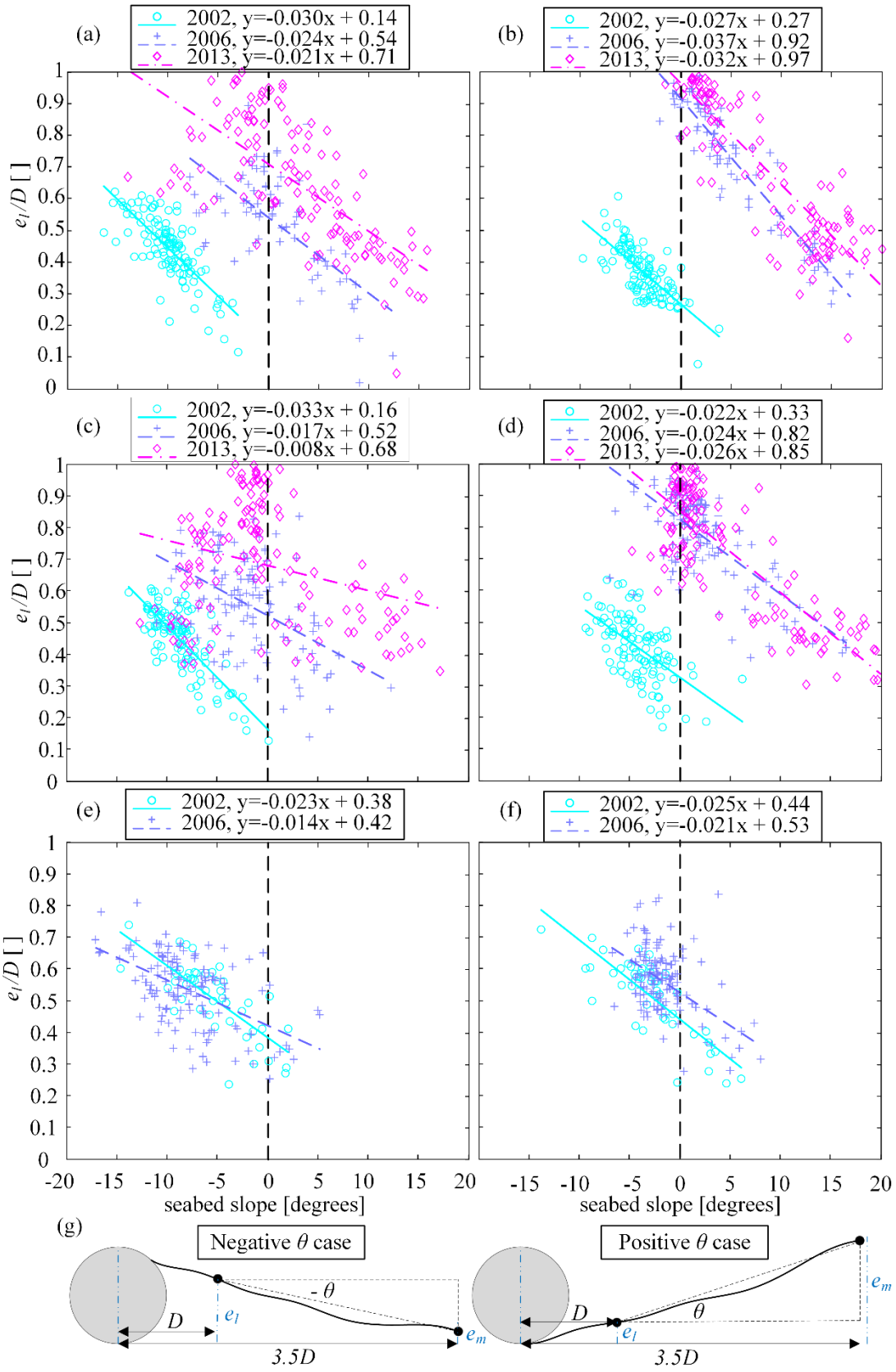

Figure 6: Relationship between local embedment and seabed slope for embedded sections of pipeline on the (a) port (offshore) and (b) starboard (onshore) sides of the section KP 7.2 – 7.4, (c) port and (d) starboard for KP 13.3 – 13.5 a€(e) port and (f) starboard for 19.9 – 20.1. Seabed slope is as defined in (g).

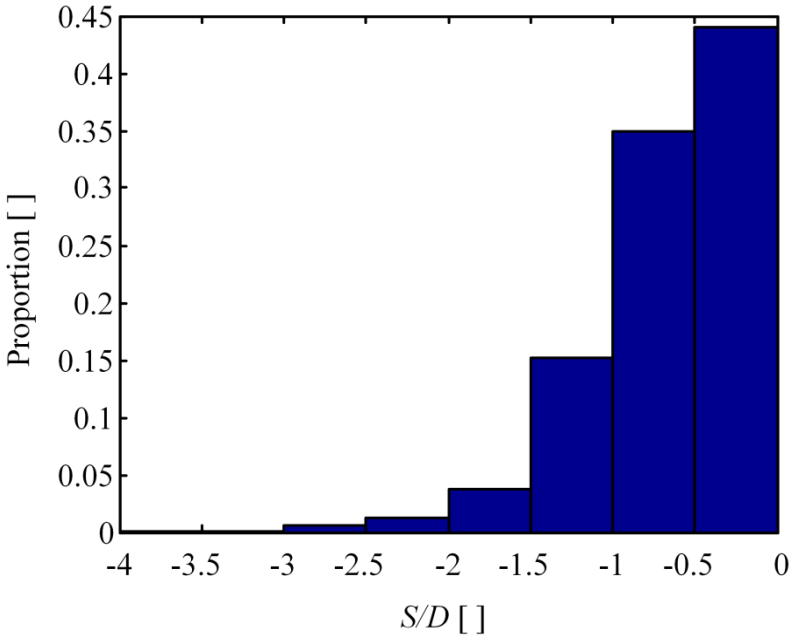

Figure 7: Histogram of the normalised scour hole depth in 2013.

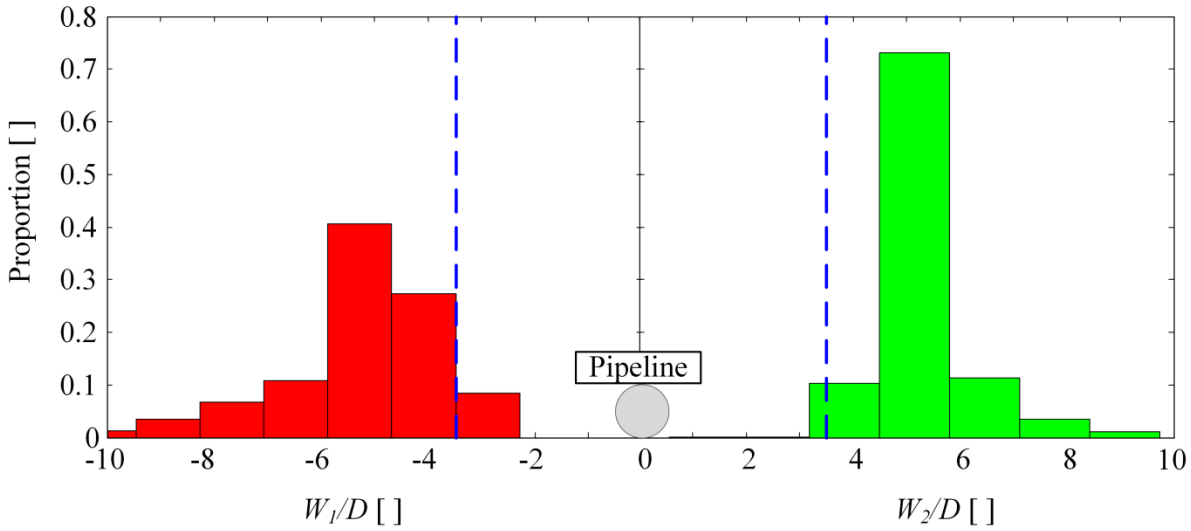

Figure 8: Histogram of scour half-width on the port (W_1) and starboard (W_2) sides of the pipeline. The vertical dashed line at 3.5*D* corresponds to the '3*D*' offset distance in the definition used in DNV RP-F105.

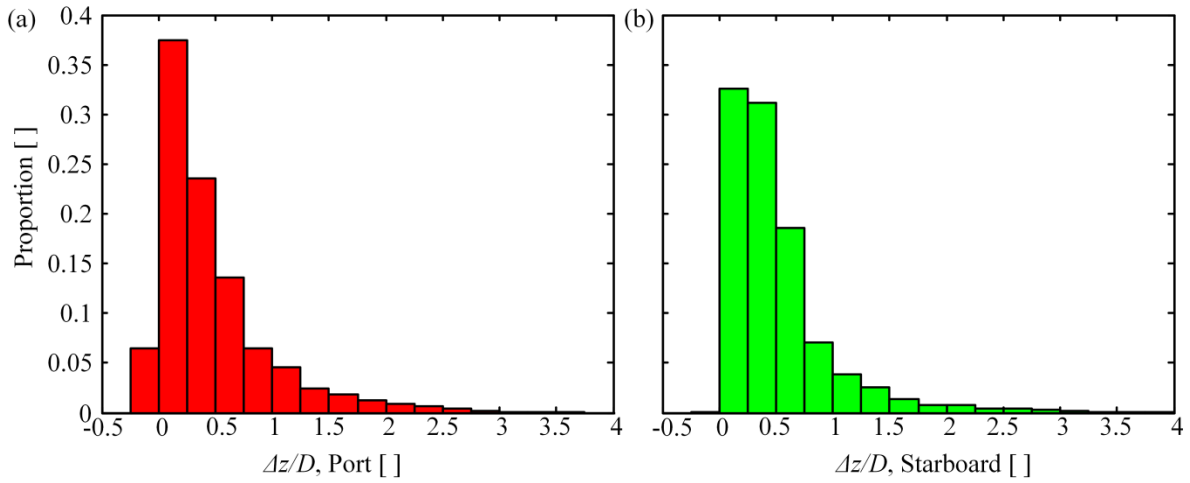

Figure 9: Histogram of the normalised difference between the seabed level at the edge of the scour hole and the seabed level at an offset of 3.5*D*. Positive values show that the embedment at the edge of the span is higher than the embedment at 3.5*D*, indicating cases where the method set out in DNV-F105 is likely to underestimate the degree of sheltering.

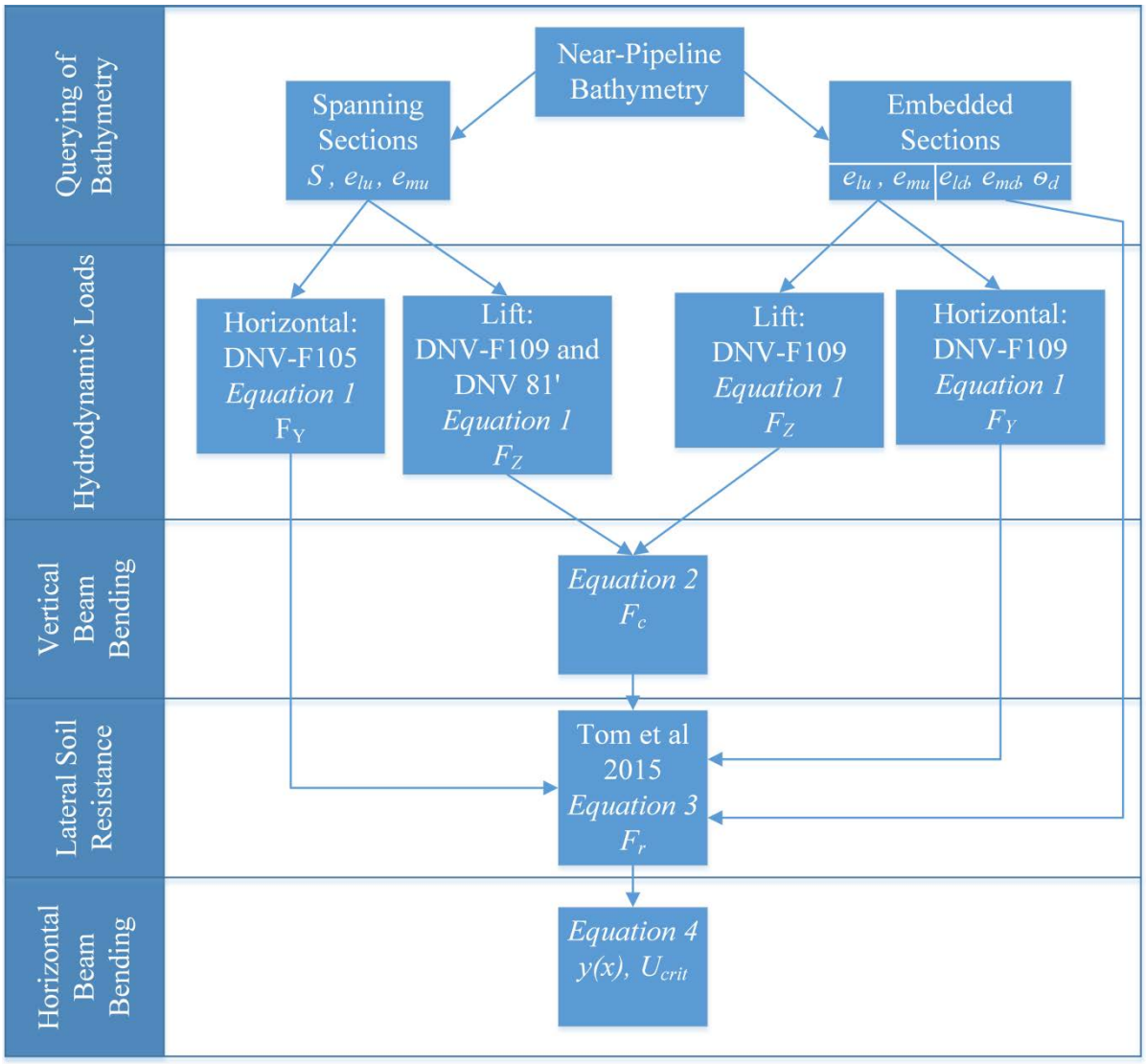

Figure 10: Structure of the stability algorithm including the design codes and equations used, and the parameters produced, at each stage.

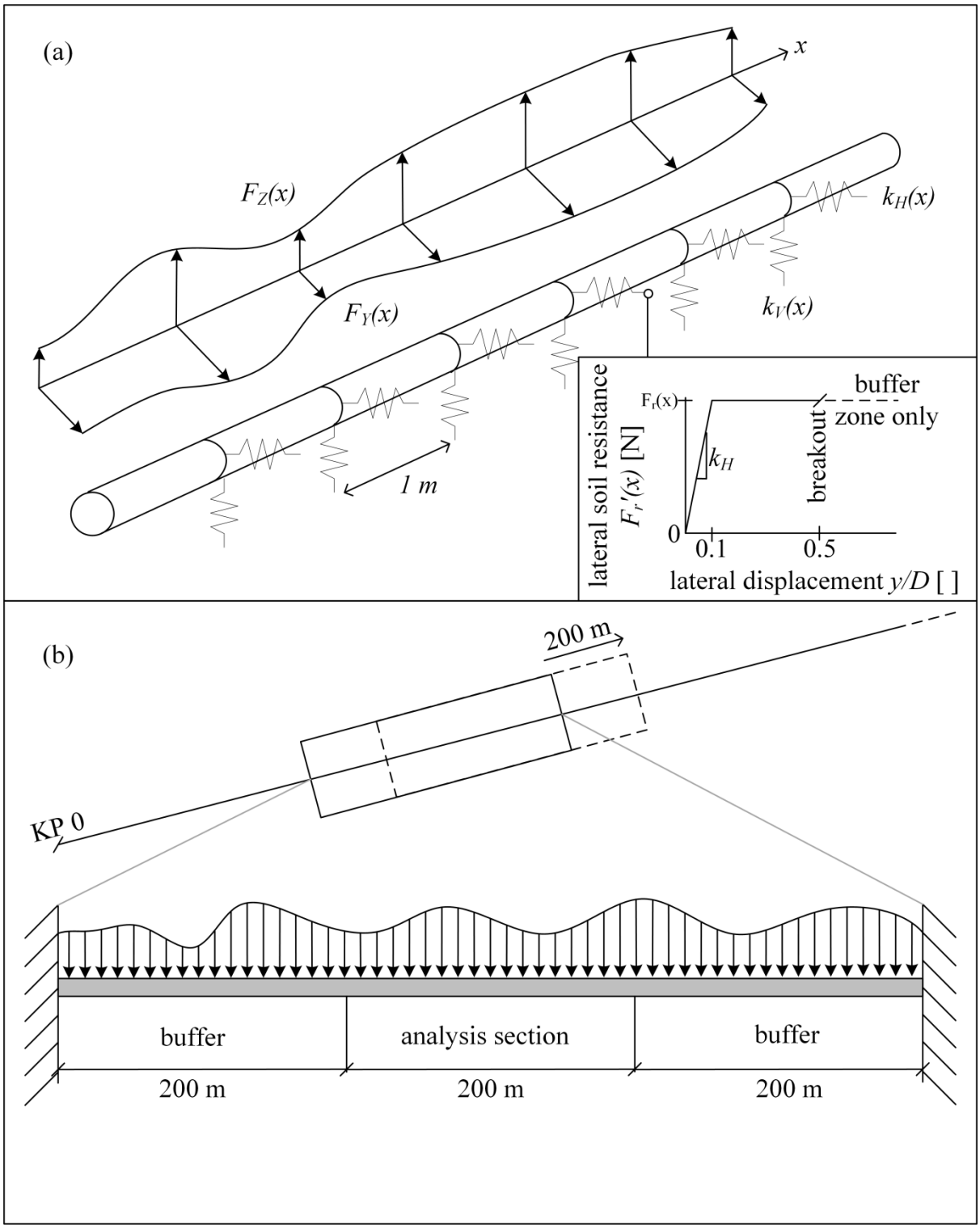

Figure 11: Schematic of the beam-bending approach showing (a) the pipe-soil interaction model and (b) the moving window approach to the beam bending solution.

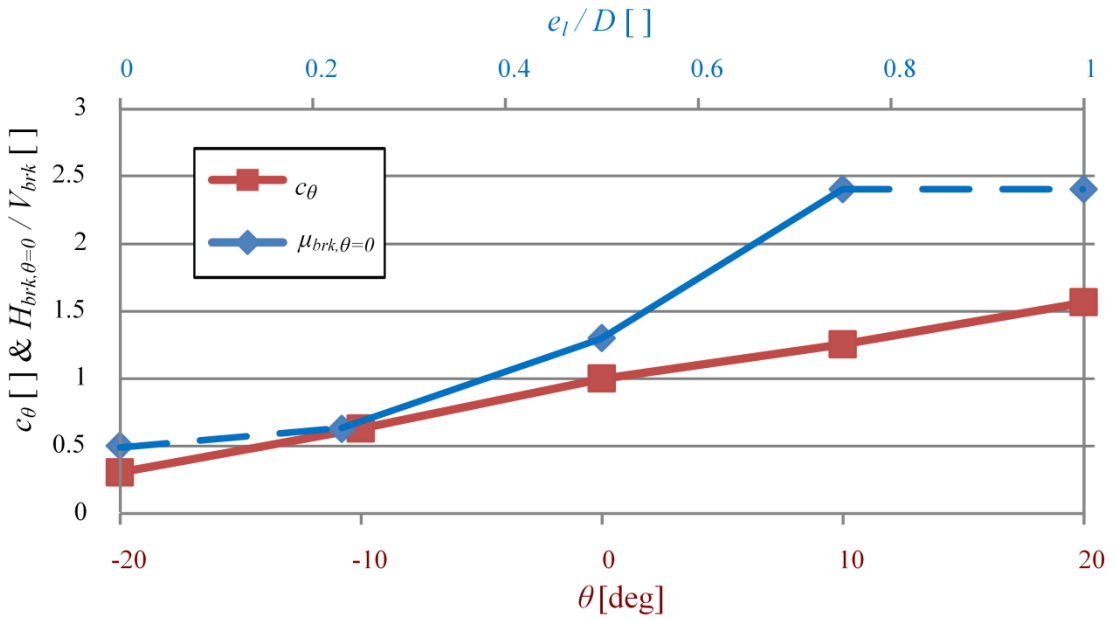

Figure 12: Available soil resistance as a function of local embedment ($\mu_{brk,\theta=0}$) and seabed slope (c_θ). The solid lines are reproduced from Tom et al. (2015) while extrapolations for this work are shown as dashed lines.

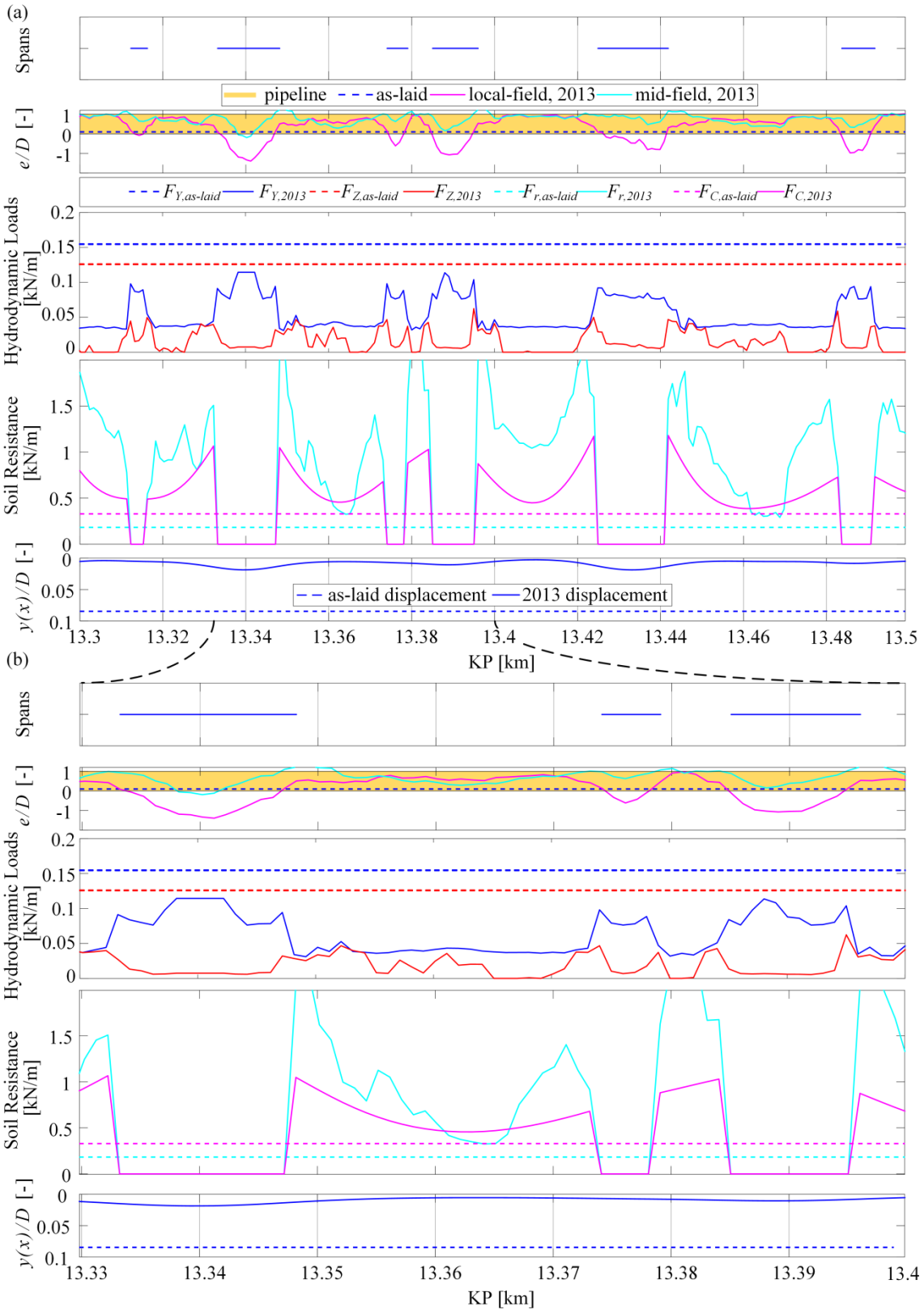

Figure 13: Variation of spanning, embedment, hydrodynamic lateral load (F_Y), lift load (F_Z), contact force (F_c), available soil resistance (F_r) and deflected profile for the as-laid and 2013 embedment condition under an offshore load of 1 m/s between (a) KP 13.3 – 13.5 and (b) the subset 13.33 – 13.4. The embedments are averages of the port and starboard values.

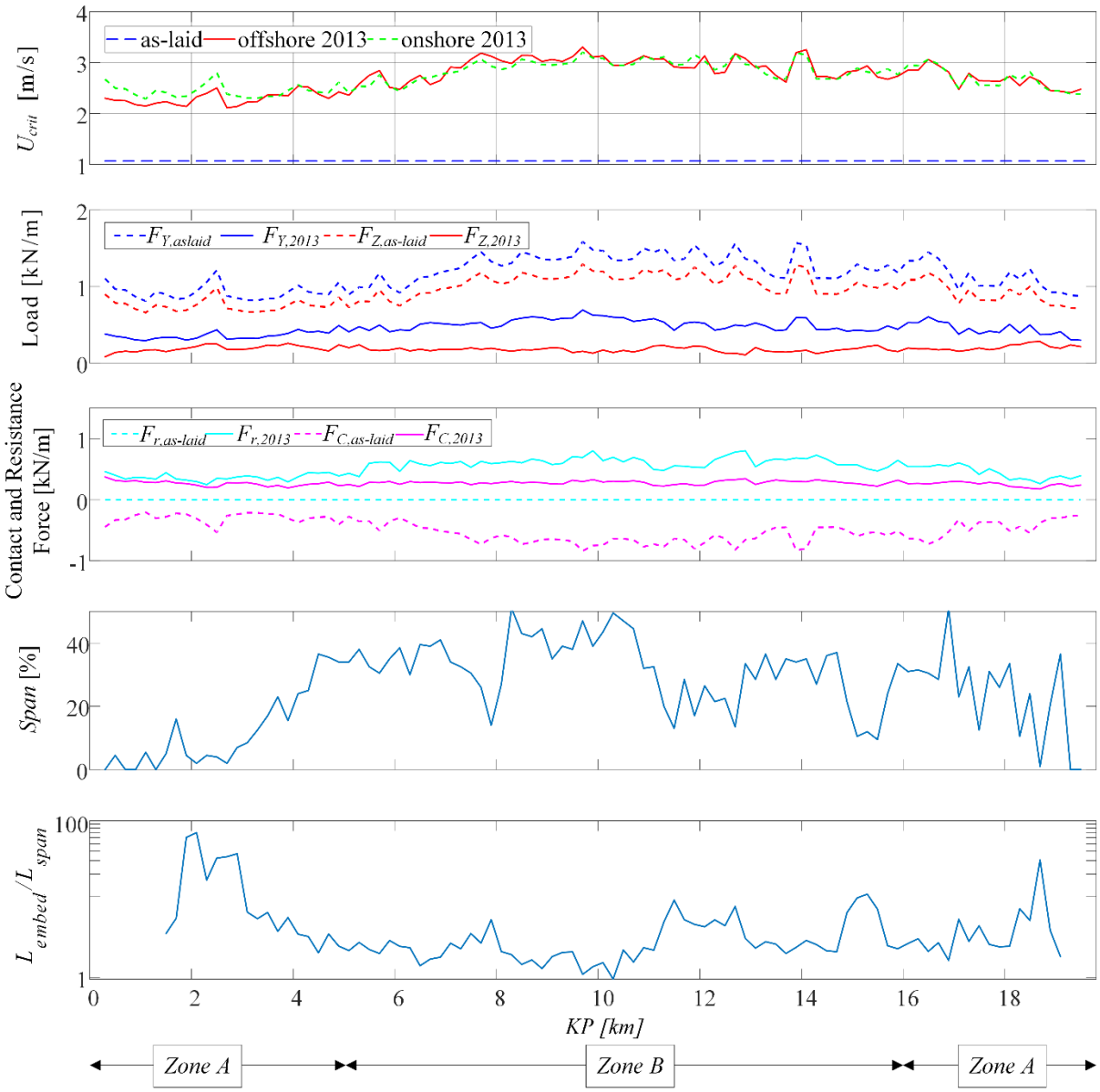

Figure 14: Critical velocity variation along the pipeline for onshore and offshore flows, hydrodynamic load, soil resistance and spanning statistics. The loads, contact and resistance values are for the 2013 offshore critical velocity case, applied to both the as-laid and 2013 seabed profiles. See text for the definition of L_{embed}/L_{span}.

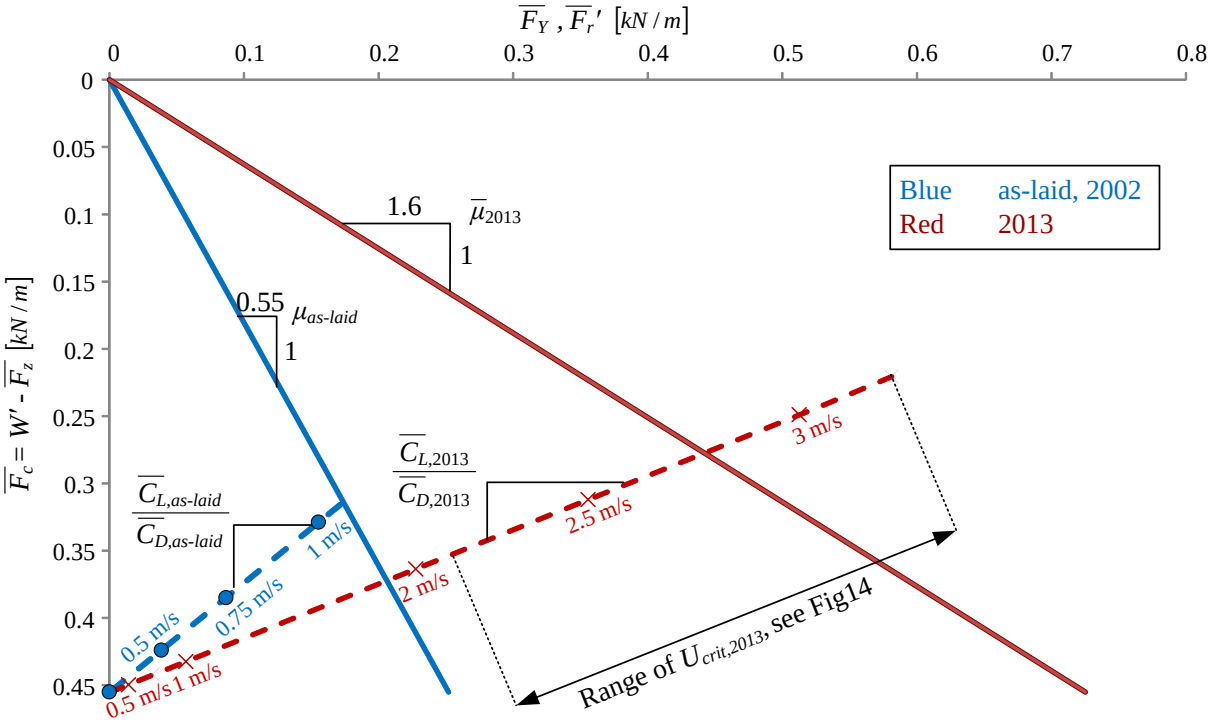

Figure 15: Failure lines (solid lines) and load paths (dashed lines) for the as-laid (blue) and 2013 (red) condition.

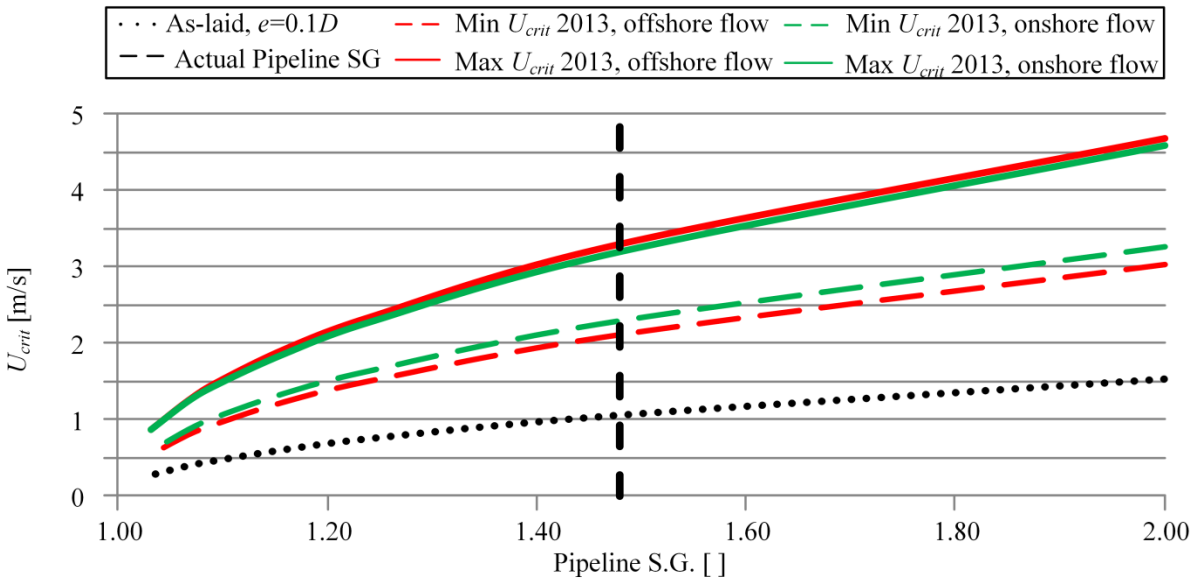

Figure 16: The influence of pipeline S.G. on critical velocity along the full surveyed length of pipeline.

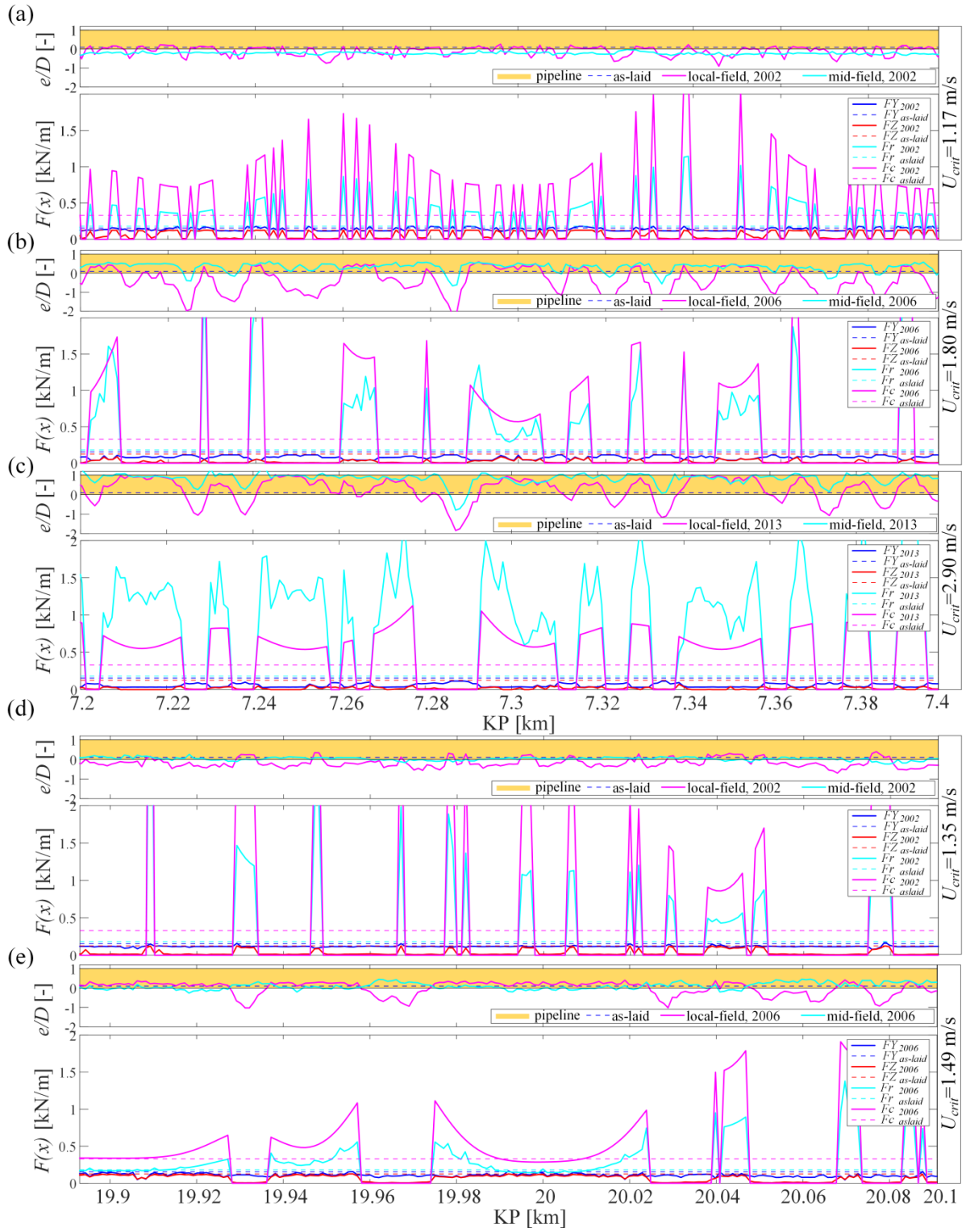

Figure 17: Changes in pipeline embedment and stability for two 200 m sections of pipeline; KP 7.2 - 7.4 in (a) 2002, (b) 2006 and (c) 2013 and KP 19.9 – 20.1 in (d) 2002 and (e) 2006.

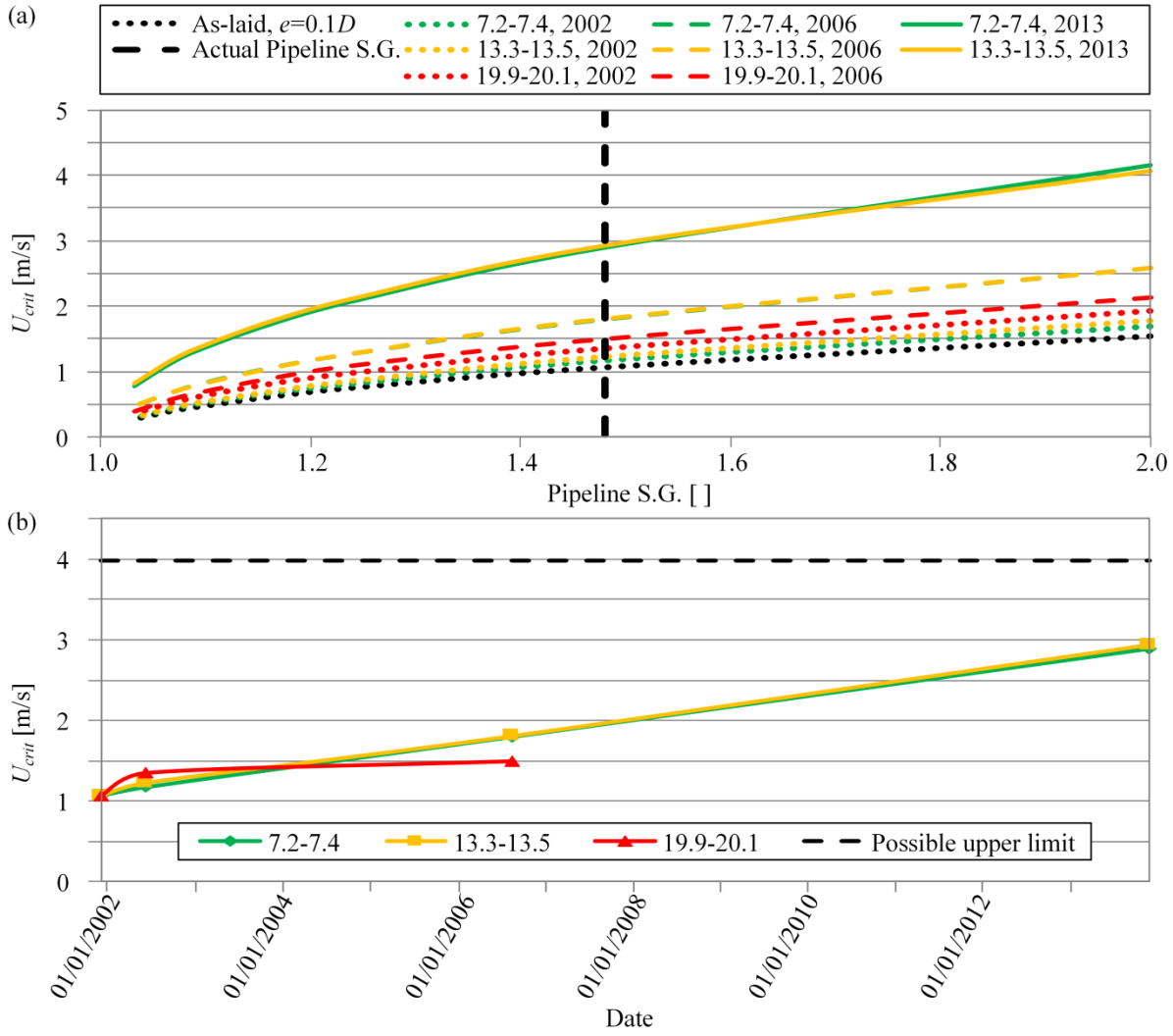

Figure 18: Stability changes with time; (a) the change in the critical velocity with time for three different sections of pipeline, (b) the change in critical velocity with time with the actual pipeline S.G. of 1.48.